Electronic Supplementary Material (ESI) for Polymer Chemistry.
This journal is © The Royal Society of Chemistry 2022

Supporting Information: Role of chain architecture on the solution phase assembly and thermoreversibility of aqueous PNIPAM/silyl methacrylate copolymers

Jason D. Linn, Lucy Liberman, Christopher A. P. Neal, and Michelle A. Calabrese*

SI.1 Materials and methods

SI.1.1 NMR of CTA

Sample for NMR spectra of 2-(ethylsulfanylthio- carbonylsulfanyl)-2-methylpropionic acid were prepared at approximately 20 mg/mL in $CDCl_3$ with a tetramethylsilane standard. The solutions were filtered through a plug of glass wool prior to analysis. The spectra were obtained on a Bruker Avance III HD 500 spectrometer equipped with a 5 mm Prodigy TCI cryoprobe. For ^{1}H spectra, 256 scans were obtained. For ^{13}C spectra, 2048 scans were obtained.

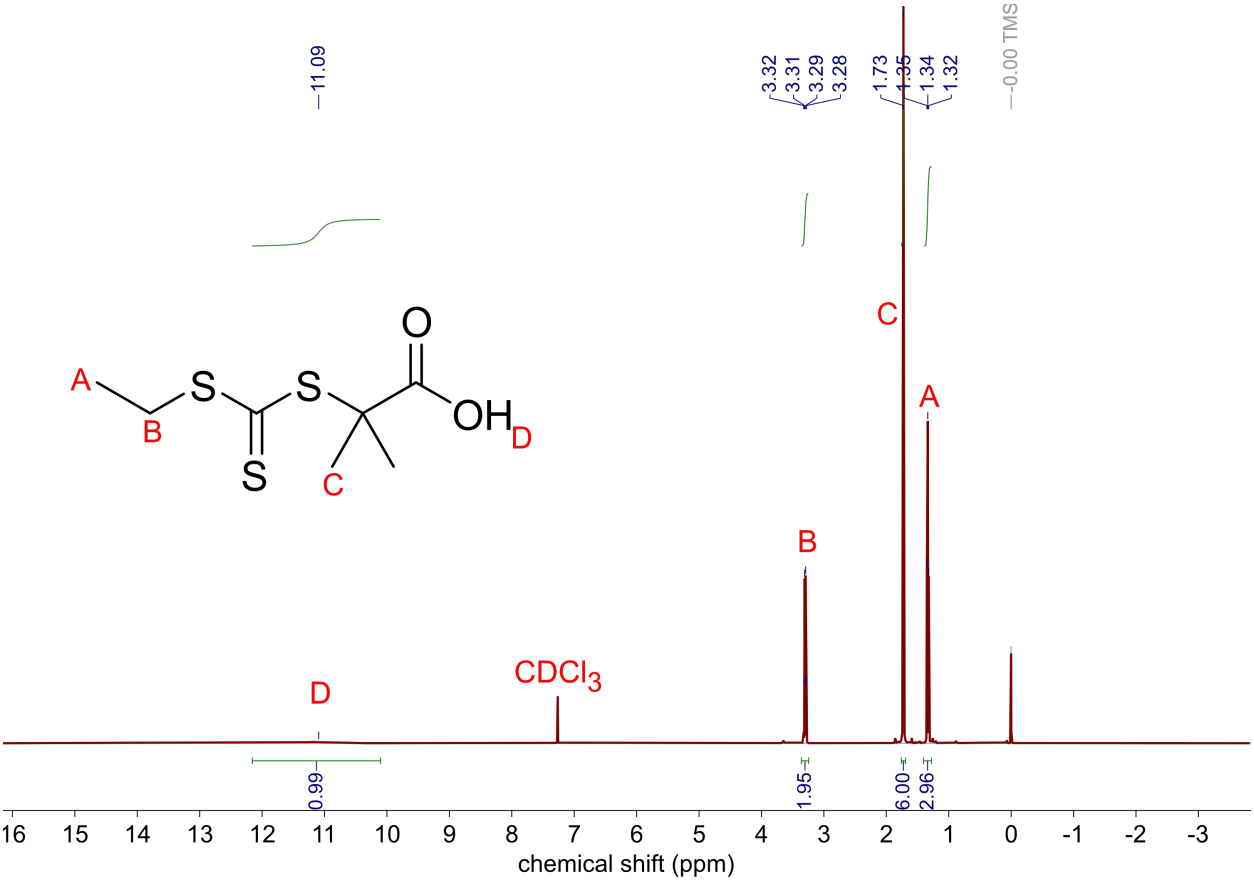

Figure S1: ^{1}H NMR of chain transfer agent 2-(ethylsulfanylthio- carbonylsulfanyl)-2-methylpropionic acid

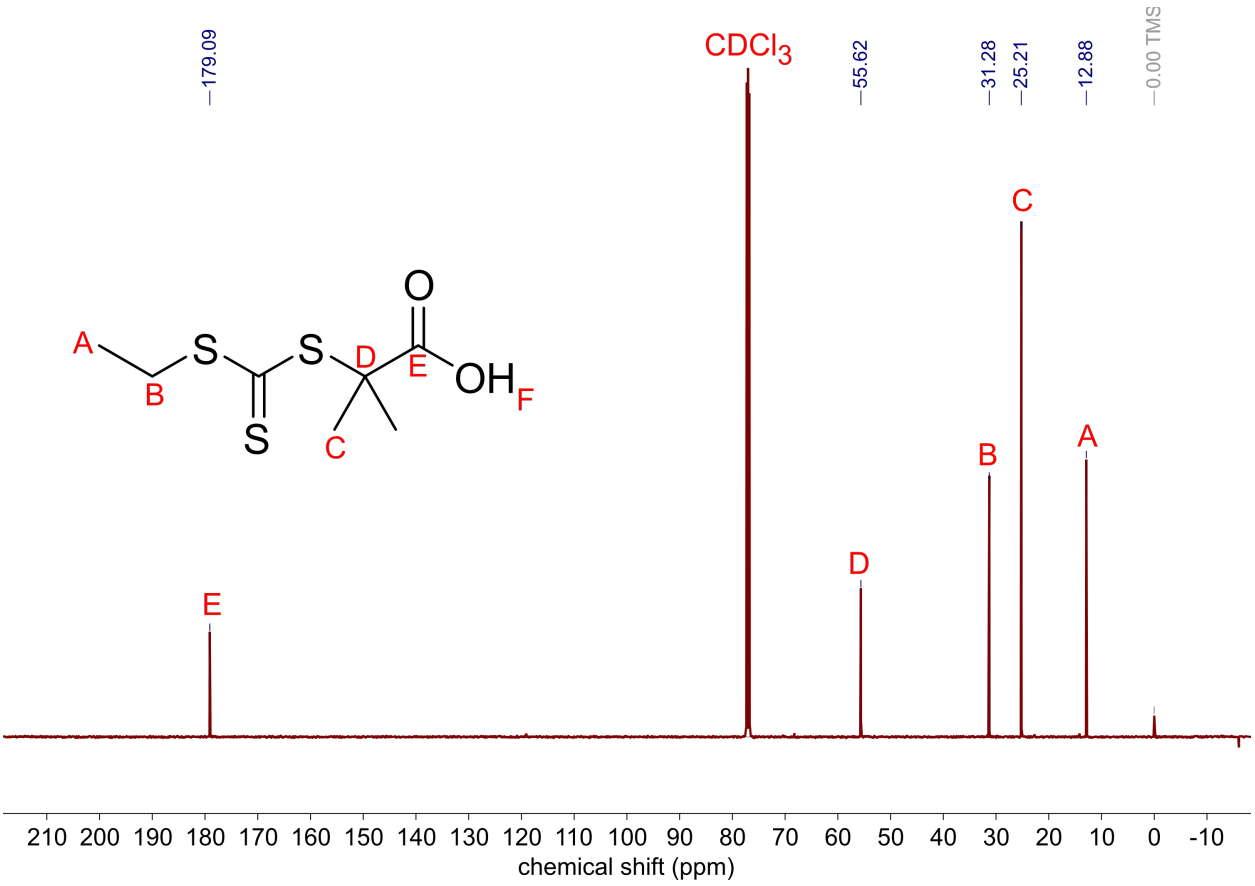

Figure S2: ^{13}C NMR of chain transfer agent 2-(ethylsulfanylthio- carbonylsulfanyl)-2-methylpropionic acid

SI.2 Polymer purification

Both copolymers and blocky-functionalized copolymers were purified following the same procedure. After quenching, the reaction mixture was diluted using approximately 10 mL of THF and stirred to lower the viscosity of the solution. This solution was then added dropwise to 800 mL of a mixture of hexanes/diethyl ether (v/v = 60/40) at -20 °C under vigorous stirring. The solid was recovered via vacuum filtration. The polymer was then redissolved in approx 20 mL of THF and precipitated once more in hexanes/ether and then filtered. The polymer was dissolved again in THF and precipitated in 800 mL petroleum ether at -20 °C. After a final vacuum filtration, the white or slightly yellow powder was dried overnight in a vacuum oven at 30 °C. The products were stored in a dessicator to reduce water uptake into the hydrophilic PNIPAM.

SI.3 Reactivity ratio calculations

SI.3.1 Q-e scheme

Using the Q-e scheme to estimate the reactivity of analogous monomers to TMA and NIPAM, methacrylate and acrylamide, yields $r_1 = 0.27$ and $r_2 = 3.6$, respectively.[1] This prediction indicates that a preferential incorporation of the acrylamide would occur at all monomer compositions.

The reactivity derive from the product of the rate constants of the different monomer species adding to chains where the propagating radical is on the different repeat units. If $r_1 > 1$, then the rate of adding monomer 1 is greater than adding monomer 2 to a chain where the propagating radical is on monomer species 1.[1] Eqn. SI.3.1 shows a simplified Mayo-Lewis equation where f corresponds to the monomer feedstock composition and F corresponds to the composition of each monomer incorporated into the copolymer. This form of the equation was used to determine the least squares fit using the MATLAB equation fitting GUI.

$$F_1 = \frac{r_1 f_1^2 + f_1 f_2}{r_1 f_1^2 + 2 f_1 f_2 + r_2 f_2^2} \tag{SI.3.1}$$

SI.3.2 Reactivity ratio reaction procedure

Prior to initiation, the reaction vessels were degassed via a free/pump/thaw process thrice. After degassing, a zero-time aliquot was withdrawn to measure the initial monomer feedstock composition, thus accounting for small measurement errors from setting up the reactions. The reactions were then lowered into an oil bath at 75 °C under vigorous stirring. Aliquots were withdrawn at regular intervals for approximately 1.5 h. Aliquots were taken using a syringe purged with inert gas. Approximately 200 μL of reaction mixture were withdrawn and deposited into 800 μL d-chloroform. The aliquots were then frozen in liquid nitrogen to quench any remaining radicals.

SI.3.3 Reaction stoichiometry and conversion of synthesized polymers

Polymer	**$[NIPAM]_0$:$[TMA]_0$:$[CTA]_0$**	**NIPAM conversion (%)**	**TMA conversion (%)**
N_{408}	500:0:1	87	N/A
N_{479}	600:0:1	88	N/A
N_{540}	883:0:1	61[a]	N/A
N_{456}/T_2	597:3:1	85	80
N_{400}/T_{14}	576:24:1	80	89
$N_{337}[N_{88}/T_3]$	594:6:1	78	63
$N_{363}[N_{113}/T_5]$	600:10.5:1	79	59
$N_{293}[N_{143}/T_8]$	585:15:1	85	81
$N_{283}[N_{113}/T_8]$	576:24:1	79	50

Table S1: Table of synthesized experimental polymers with initial reaction stoichiometry and individual monomer conversion prior to purification, as measured by ^{1}H NMR. [a]Conversion estimated by SEC-MALS of final product.

SI.3.4 NMR of polymers

SI.3.5 Procedure for NMR analysis of polymers

An AX-400 Bruker Avance III HD was used to acquire NMR spectra. For a typical 1D ^{1}H NMR spectrum, 64 or 128 scans were performed.

All NMR spectra were obtained using $CDCl_3$ as the solvent with tetramethylsilane as the NMR standard. To prepare a sample for NMR, approximately 20 mg of dried polymer was added to a vial. Then, 800 µL of deuterated solvent was added. The samples were agitated until the polymer dissolved. The solution was then filtered through glass wool packed into a pipette to remove any dust and undissolved polymer into the NMR tube.

SI.3.6 Aliquot tracking TMA/NIPAM copolymerization using ^{1}H NMR

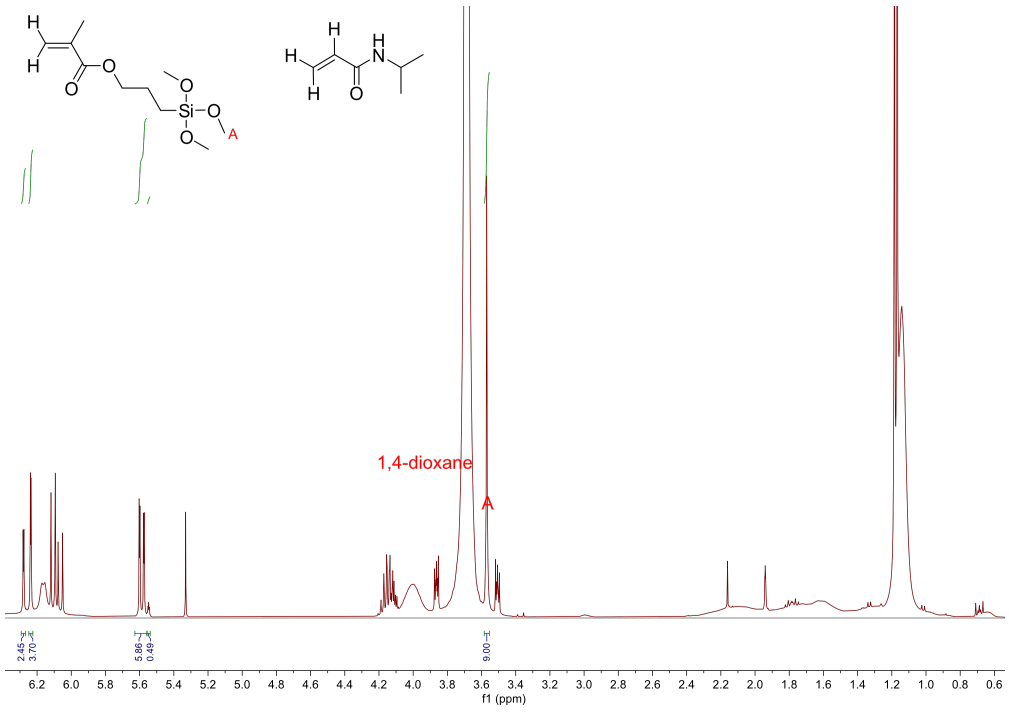

Figure S3: TMA/NIPAM copolymerization aliquot spectrum at intermediate conversion

SI.3.7 ^{1}H NMR of alkene region

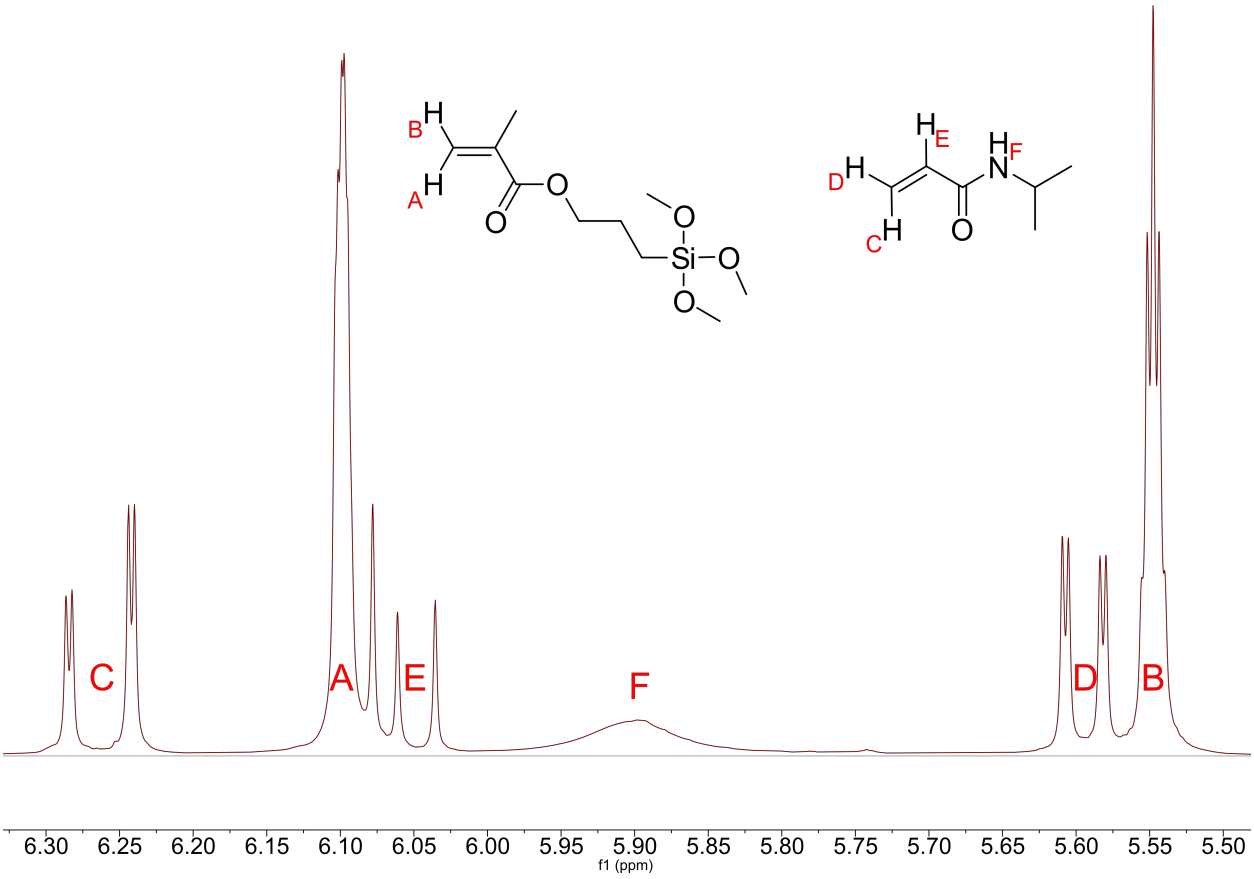

Figure S4: ^{1}H NMR of the alkene region during polymerization used to track monomer conversions.

SI.3.8 ^{1}H-^{1}H-homonuclear correlation spectroscopy (COSY) confirms alkene peak assignments in TMA/NIPAM copolymerization

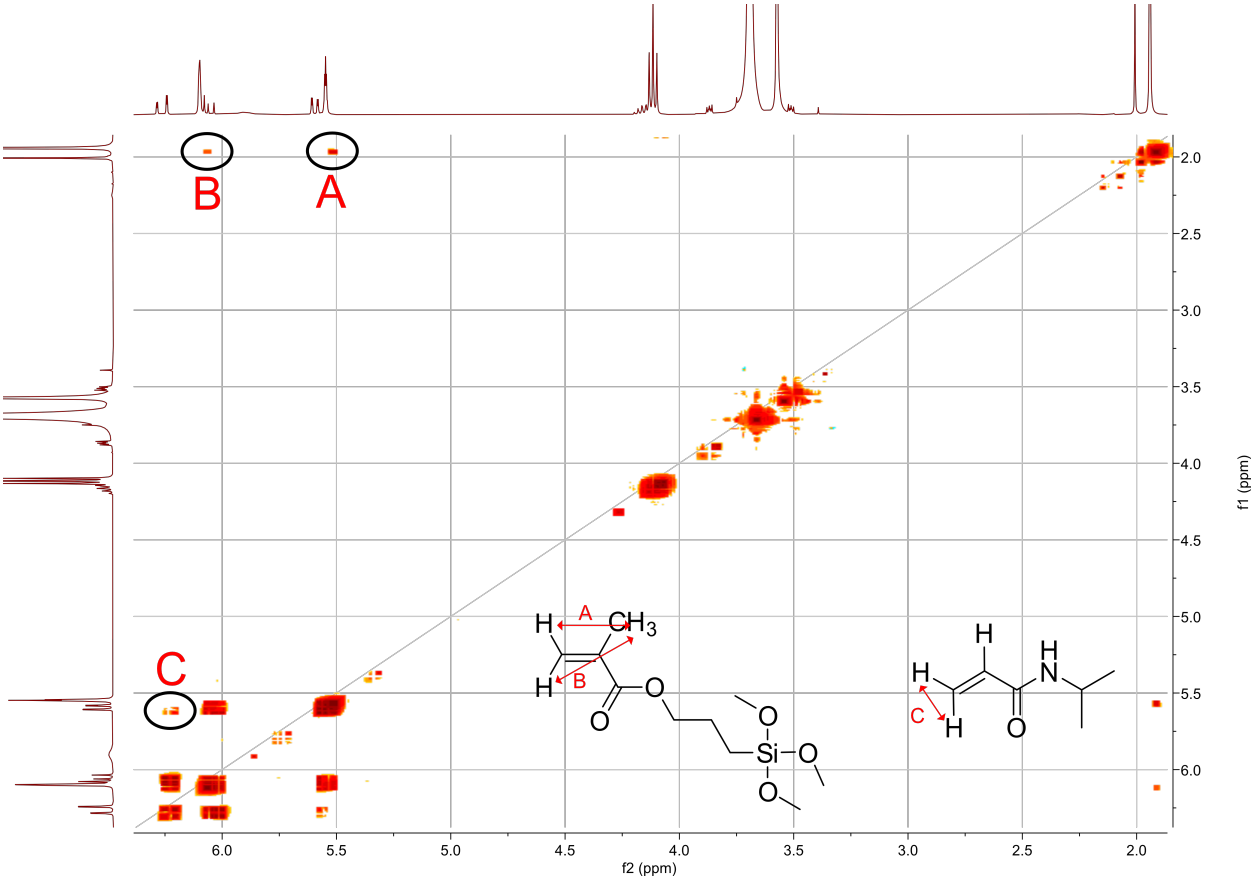

Figure S5: COSY NMR confirms the alkene region assignments through correlated cross peaks. Spectrum obtained in $CDCl_3$.

COSY NMR relates protons through carbon-carbon bonds. The center diagonal is essentially a normal ^{1}H NMR spectrum, and off diagonal peaks indicate couplings between protons. In the above spectrum, the peaks labelled A and B show the correlations between the methyl and the methylene protons on the TMA monomer. Peak C is the correlation between the two methylene protons in NIPAM. These findings support the aforementioned assignments and suggest that the discussed integrations are be reproducible.

SI.3.9 HSQC NMR confirms the overlap of two peaks in P(NIPAM-*co*-TMA) integration

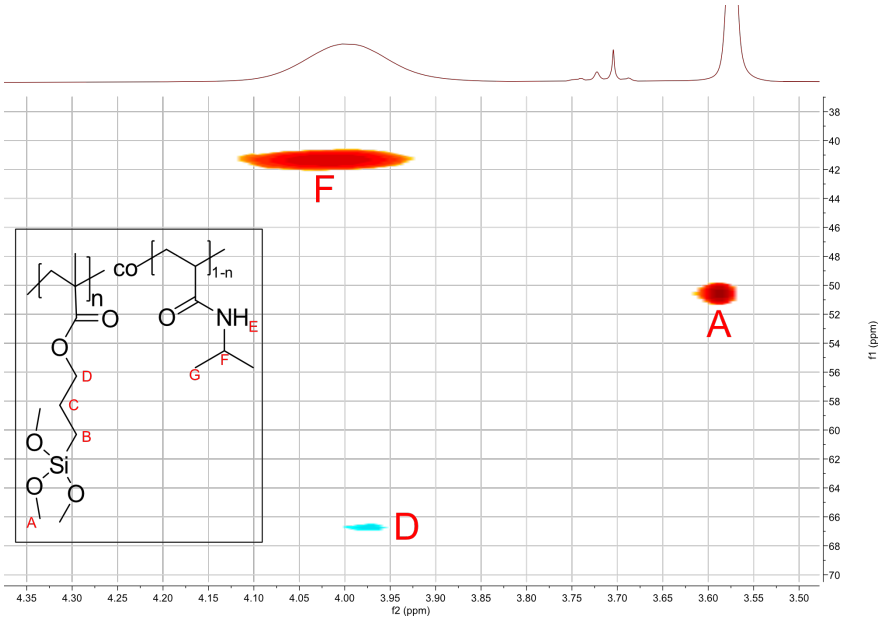

Figure S6: HSQC NMR confirms the overlap of two peaks in P(NIPAM-*co*-TMA) integration.

SI.4 ^{1}H and ^{13}C NMR of polymers

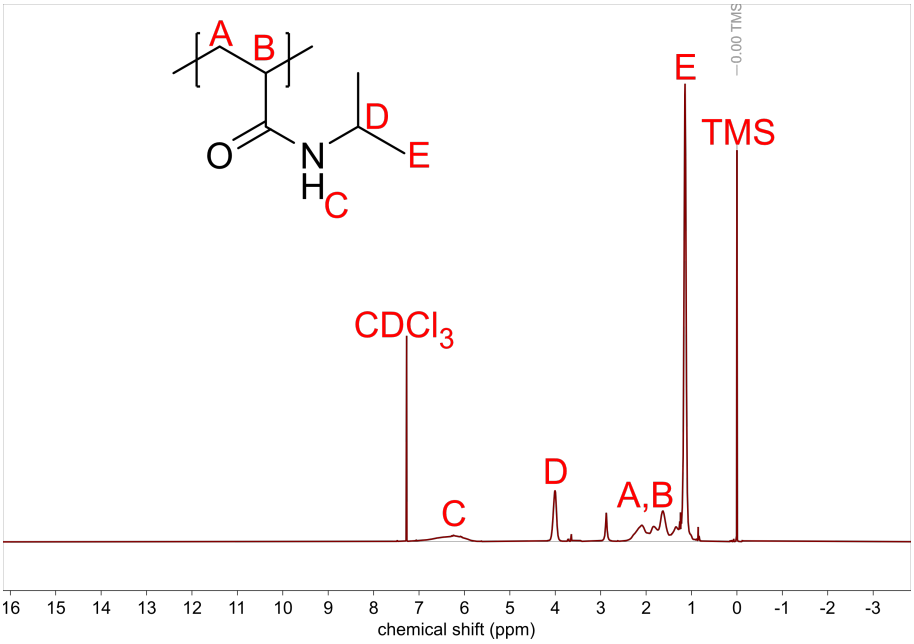

Figure S7: N_{408} ^{1}H NMR

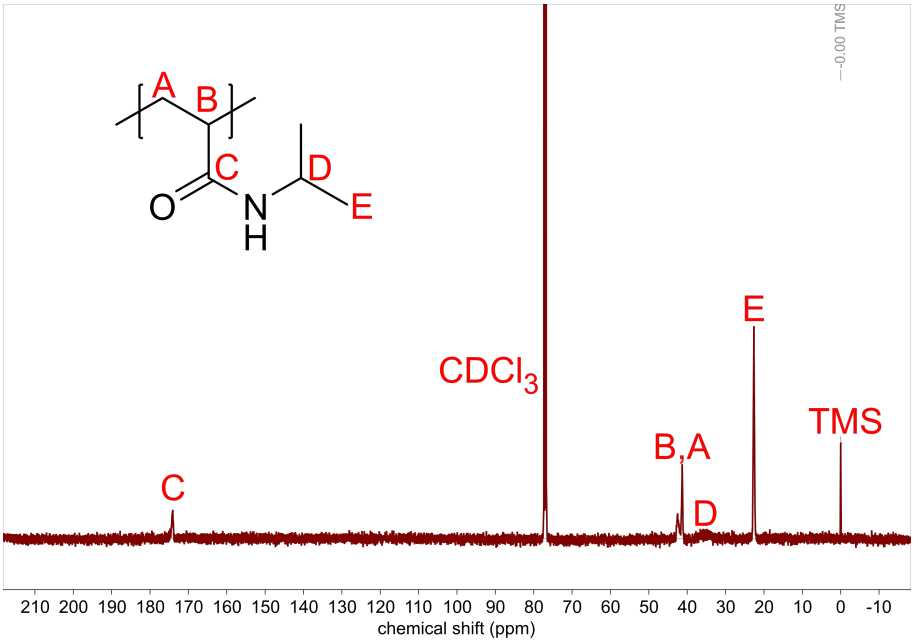

Figure S8: N_{408} ^{13}C NMR

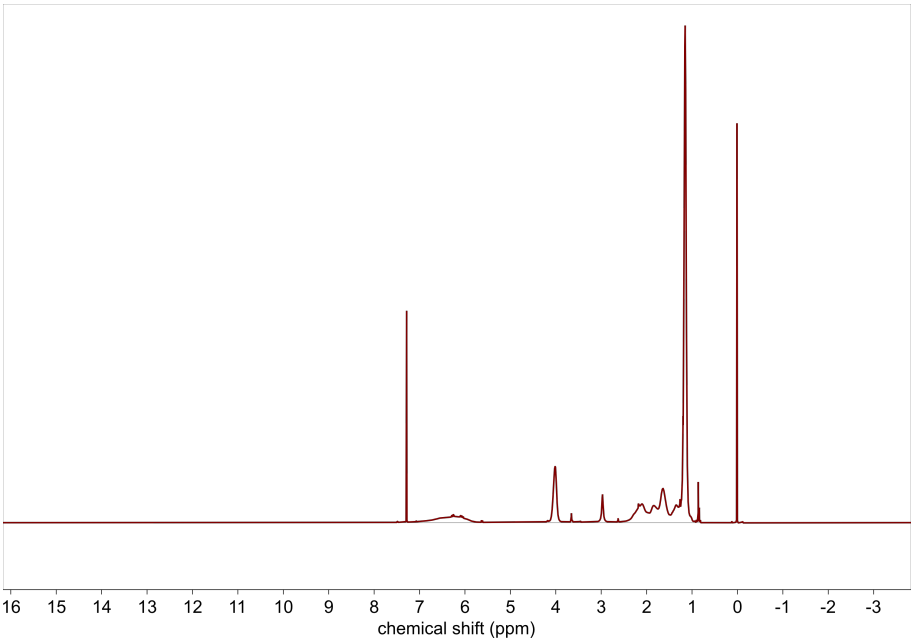

Figure S9: N_{479} ^{1}H NMR. Peak assignments identical to S7.

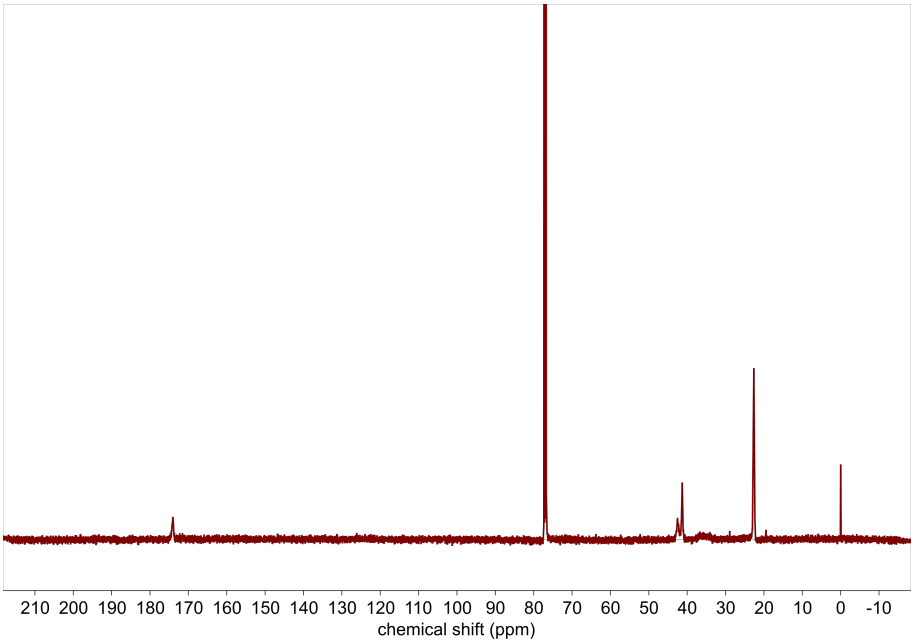

Figure S10: N_{479} ^{13}C NMR. Peak assignments identical to S8

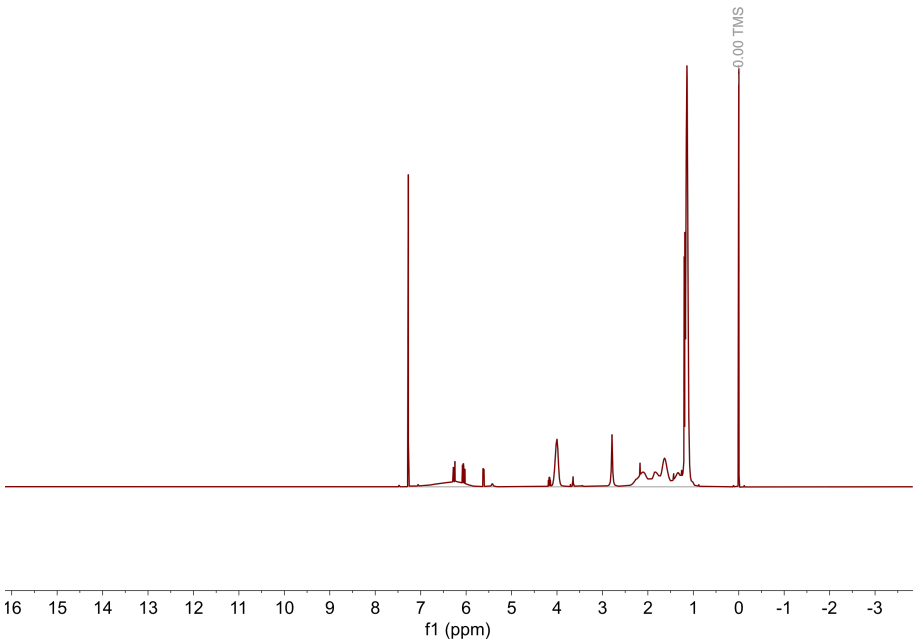

Figure S11: N_{540} ^{1}H NMR. Peak assignments identical to S7.

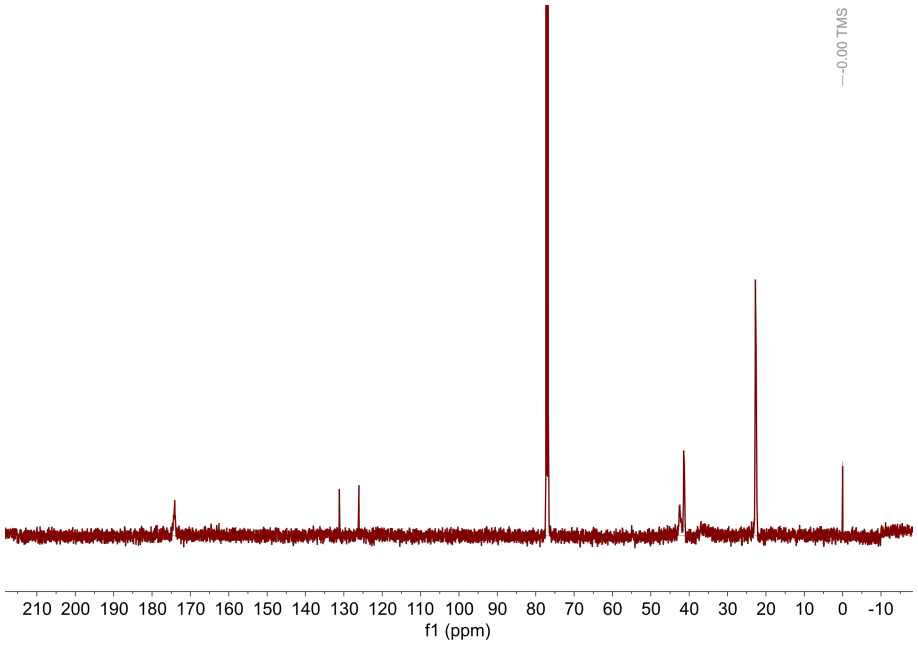

Figure S12: N_{540} ^{13}C NMR. Peak assignments identical to S8. Peaks between 120-140 ppm are residual monomer.

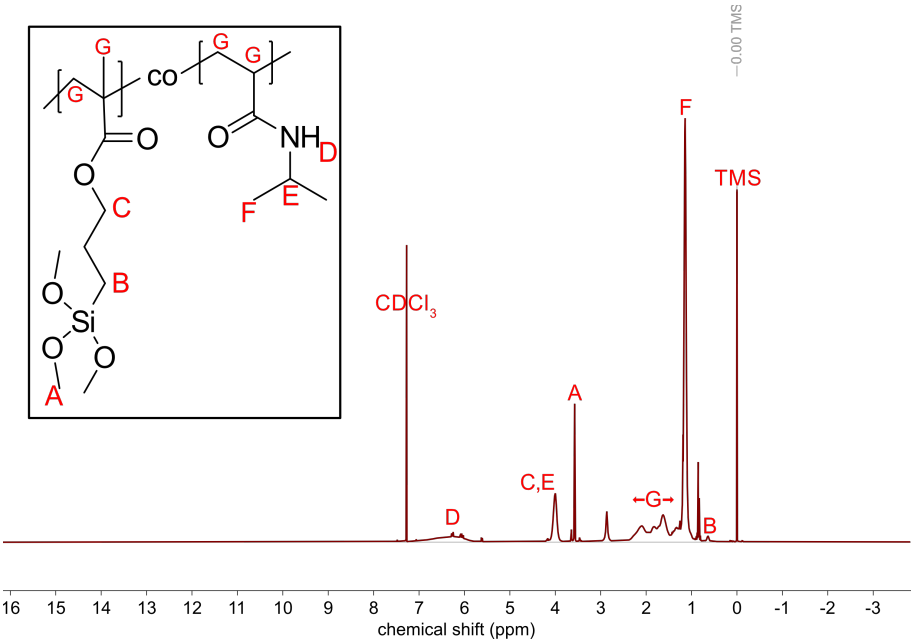

Figure S13: N_{400}/T_{14} ^{1}H NMR.

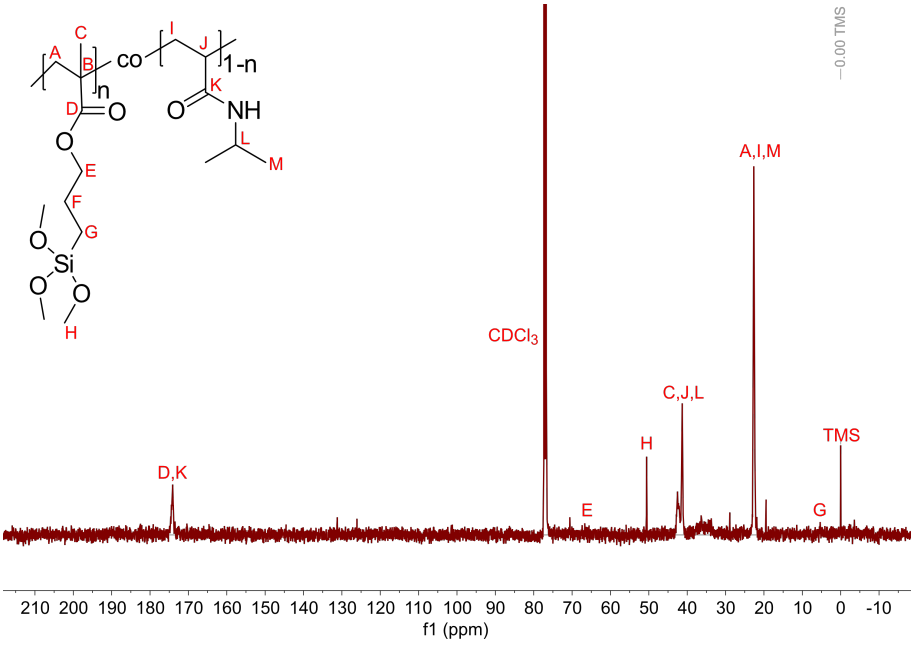

Figure S14: N_{400}/T_{14} ^{13}C NMR.

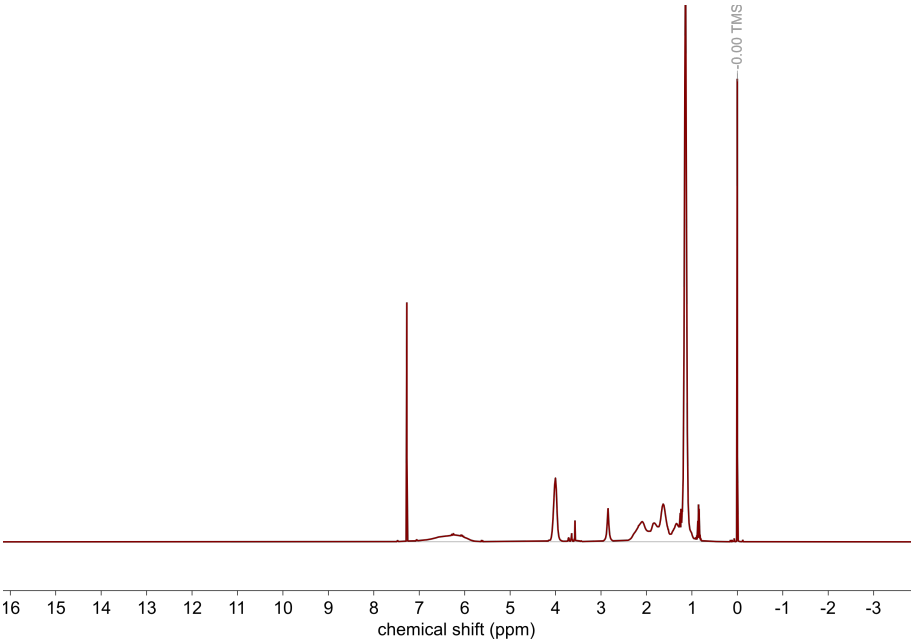

Figure S15: N_{456}/T_2 ^{1}H NMR. Peak assignments identical to S13.

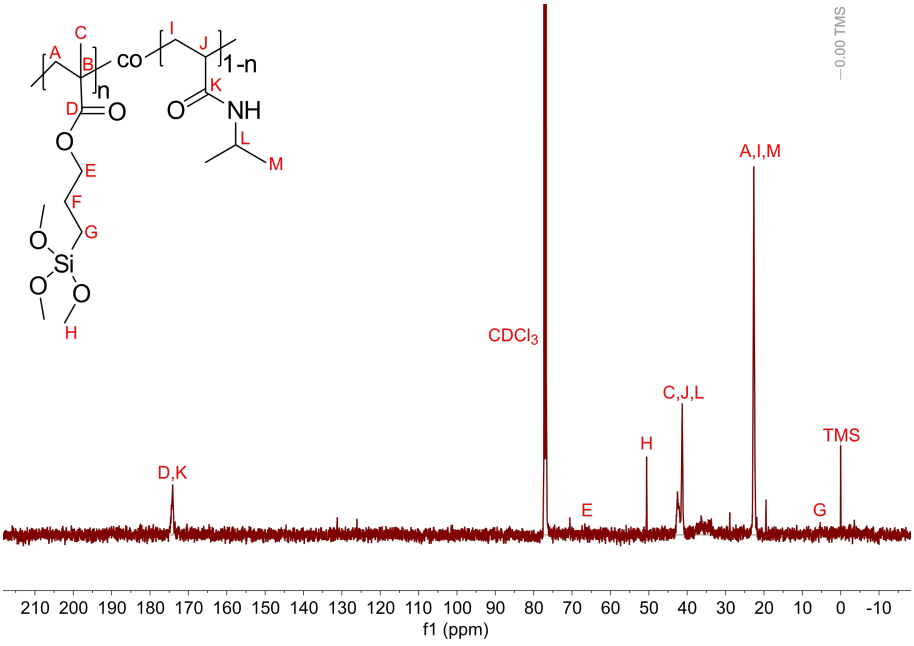

Figure S16: N_{456}/T_2 ^{13}C NMR. Peak assignments identical to S14.

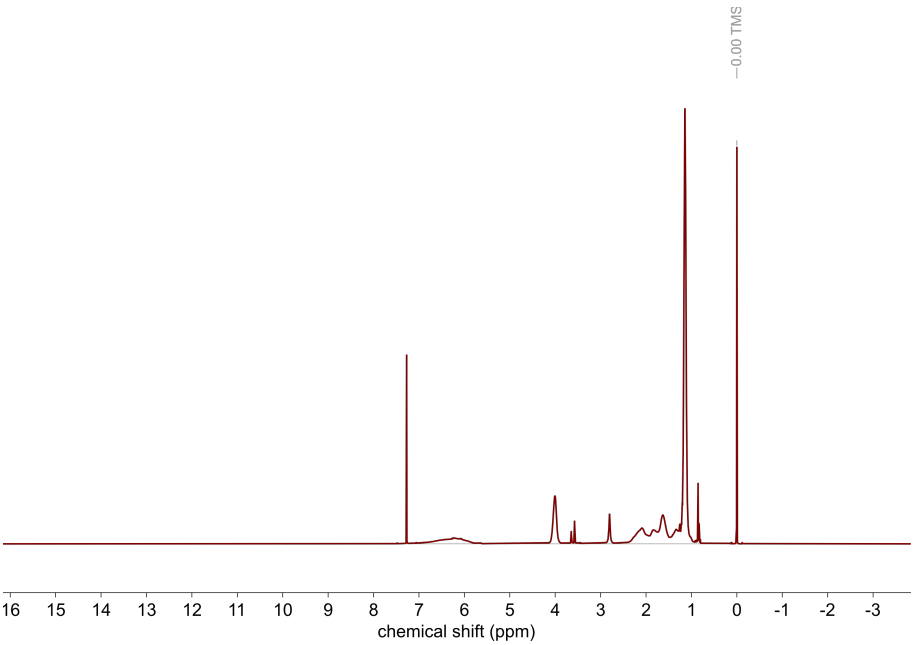

Figure S17: $N_{337}[N_{88}/T_3]$ ^{1}H NMR. Peak assignments identical to S13.

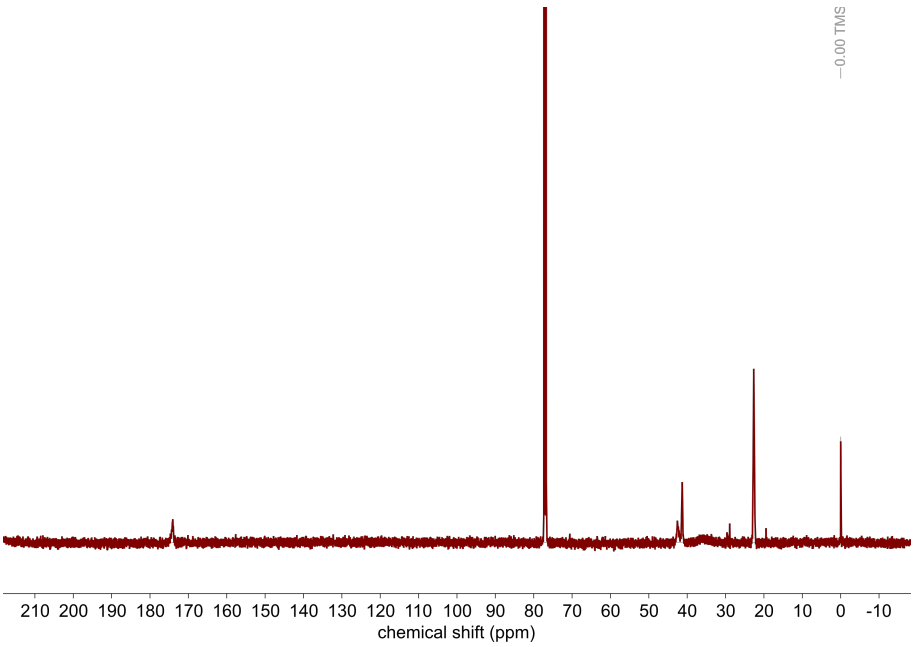

Figure S18: $N_{337}[N_{88}/T_3]$ ^{13}C NMR. Peak assignments identical to S14.

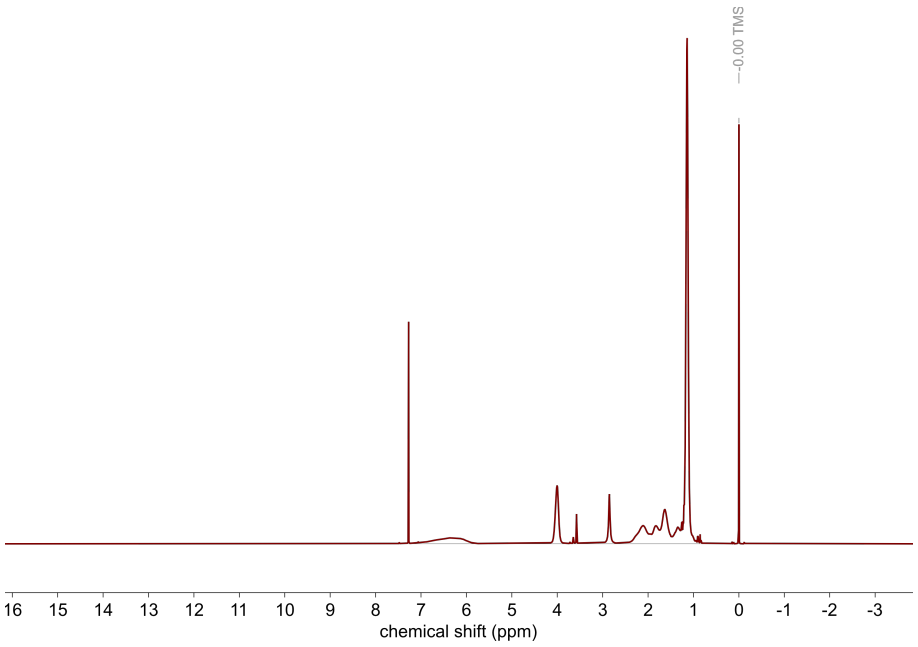

Figure S19: $N_{363}[N_{113}/T_5]$ ^{1}H NMR. Peak assignments identical to S13.

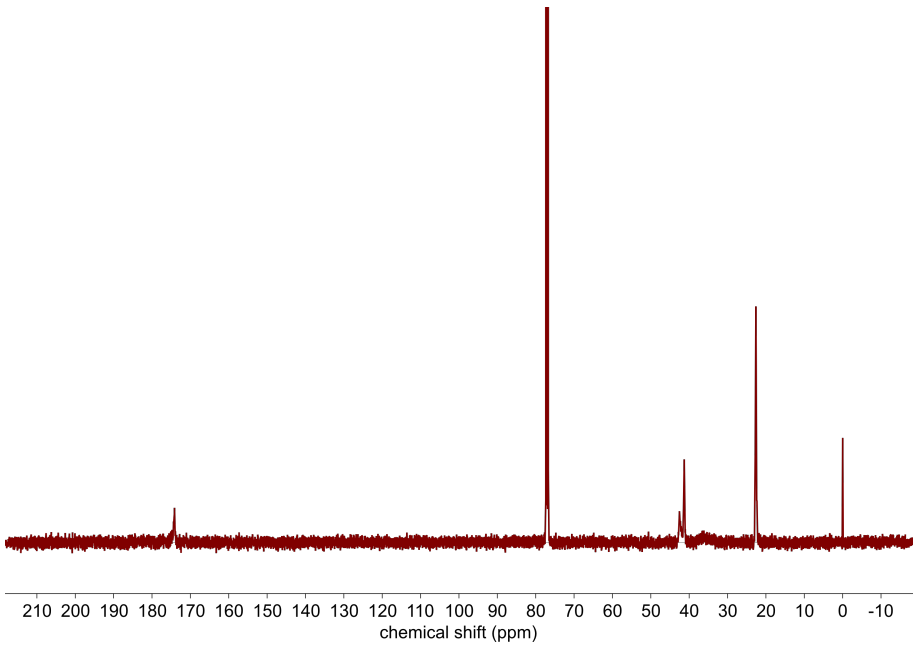

Figure S20: $N_{363}[N_{113}/T_5]$ ^{13}C NMR. Peak assignments identical to S14.

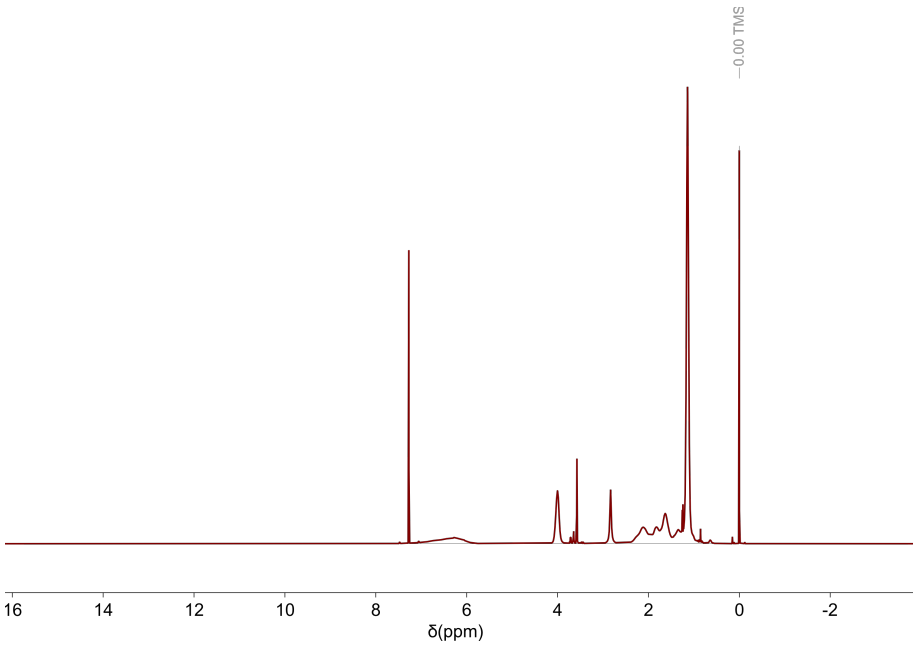

Figure S21: $N_{293}[N_{143}/T_8]$ ^{1}H NMR. Peak assignments identical to S13.

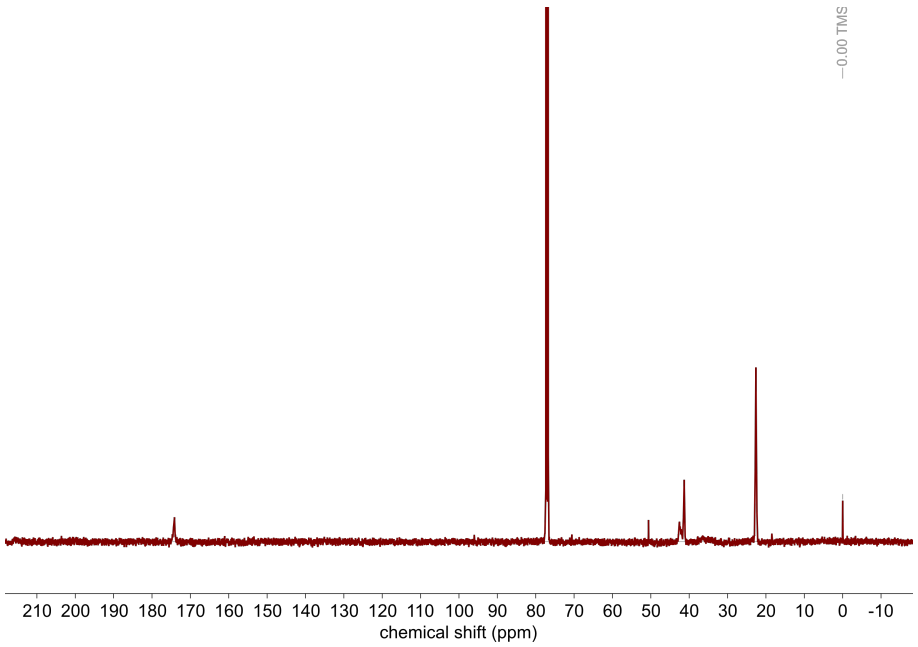

Figure S22: $N_{293}[N_{143}/T_8]$ ^{13}C NMR. Peak assignments identical to S14.

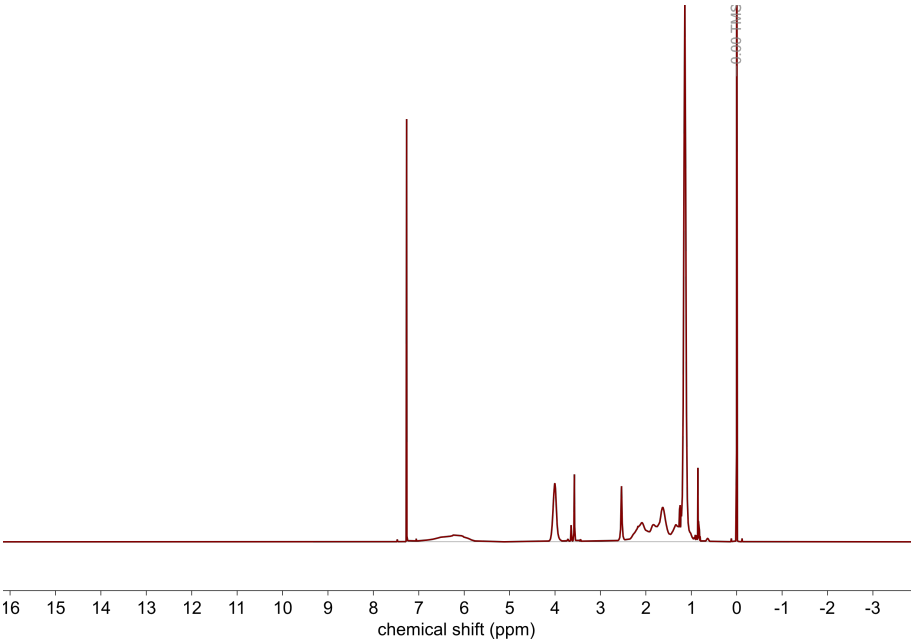

Figure S23: $N_{283}[N_{113}/T_8]$ ^{1}H NMR. Peak assignments identical to S13.

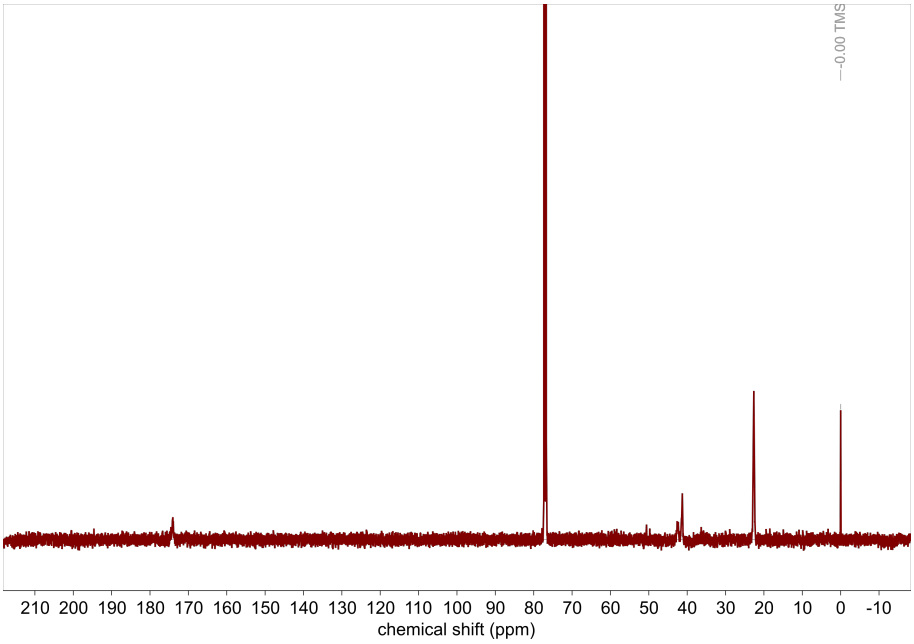

Figure S24: $N_{283}[N_{113}/T_8]$ ^{13}C NMR. Peak assignments identical to S14.

SI.5 SEC traces

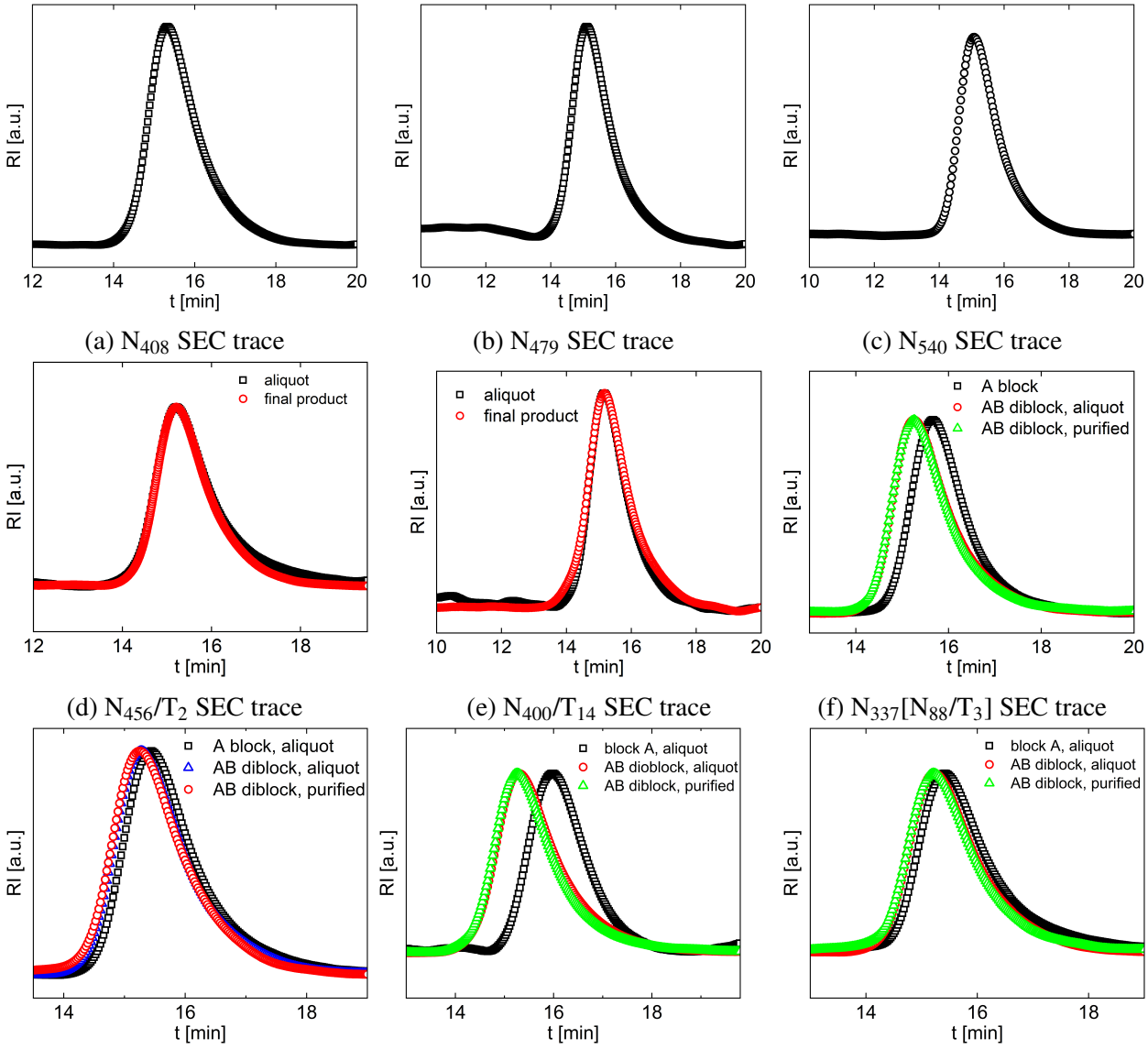

(a) N_{408} SEC trace (b) N_{479} SEC trace (c) N_{540} SEC trace

(d) N_{456}/T_2 SEC trace (e) N_{400}/T_{14} SEC trace (f) $N_{337}[N_{88}/T_3]$ SEC trace

(g) $N_{363}[N_{113}/T_5]$ SEC trace (h) $N_{293}[N_{143}/T_8]$ SEC trace (i) $N_{283}[N_{113}/T_8]$ SEC trace

Figure S25: SEC traces of synthesized products reported in main text.

SI.5.1 SEC traces of polymers with higher F_{TMA}

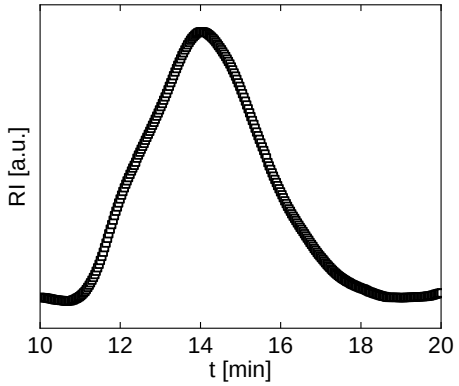

Figure S26: SEC trace of PNIPAM-co-TMA copolymer ($F_{\text{TMA}} = 7.7\%$ mol, $M_{\text{n}} = 170$ kDa, Đ= 4.3)

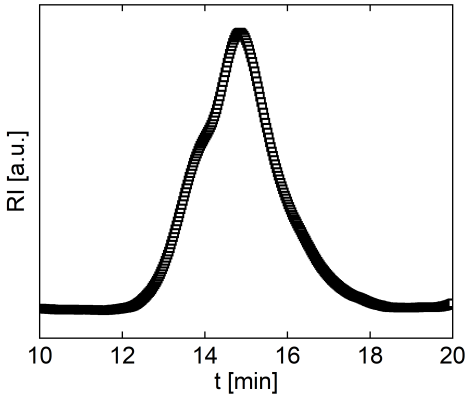

Figure S27: SEC trace of PNIPAM-co-TMA copolymer ($F_{\text{TMA}} = 10.3\%$ mol, $M_{\text{n}} = 64$ kDa, Đ= 1.8)

Copolymers containing higher TMA content demonstrate a distinct high molecular weight shoulder likely due to intermolecular crosslinking of the silanes at higher TMA incorporation. Given the goal to connect polymer chain configuration to function, minimizing silane coupling prior to experimentation was essential. As such, polymers with low TMA contents were the focus of this report.

SI.6 Dynamic light scattering (DLS) raw data

The following DLS data is organized with the raw data for each polymer presented in Figs. S28-S54. Figs. S55-S57 show data overlaid for multiple samples. Fig. S58 shows multivariate analysis between polymer structural parameters and DLS measurements.

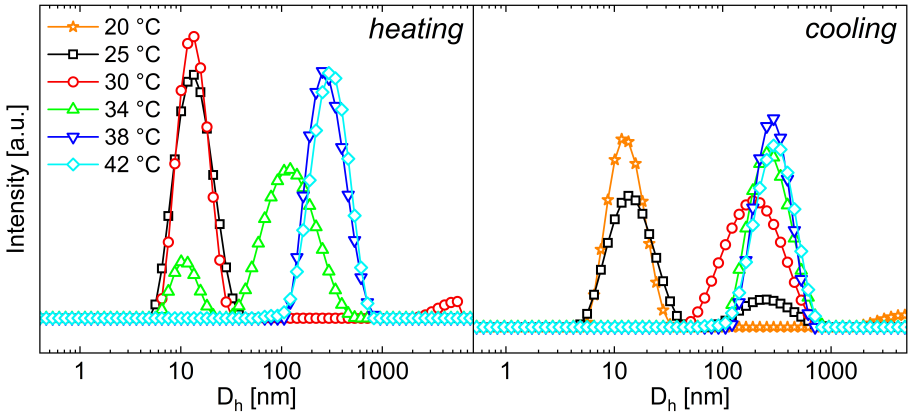

Figure S28: Intensity probability distribution of N_{408}

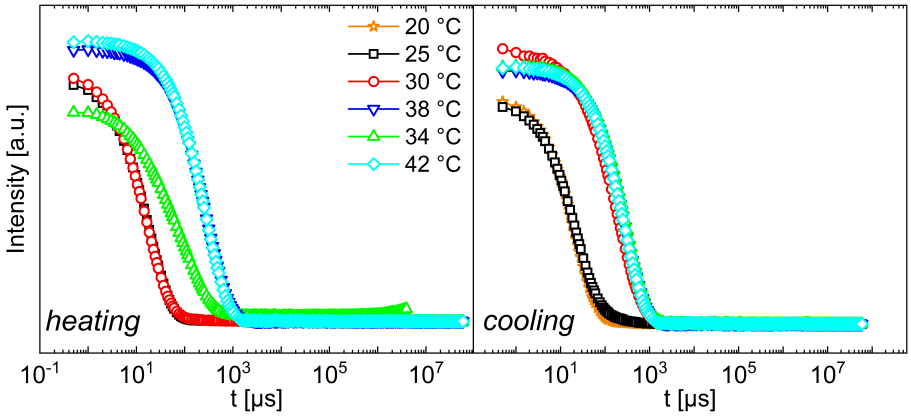

Figure S29: Autocorrelation curves of N_{408}

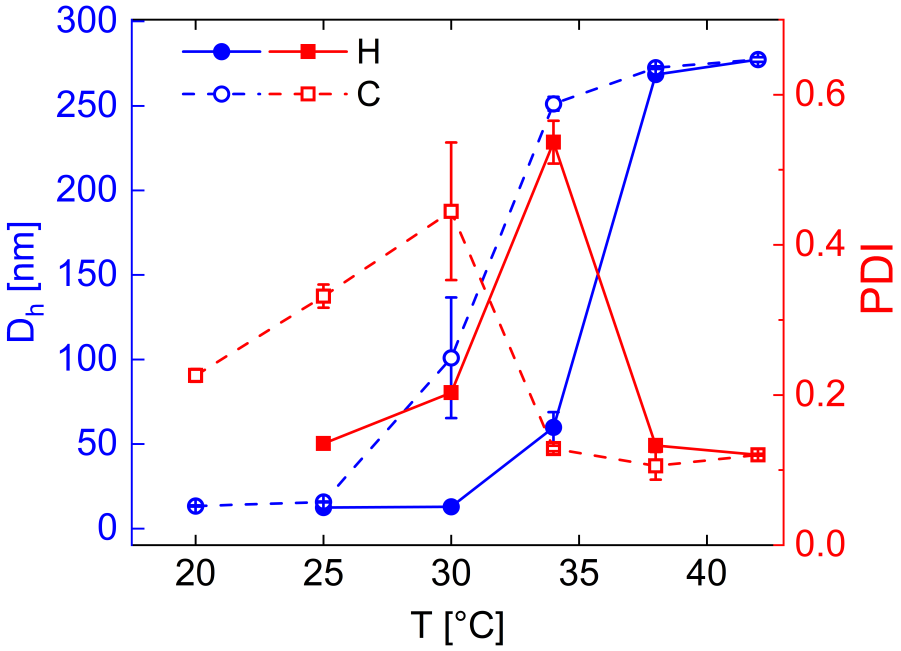

Figure S30: Size and PDI of N_{408} from DLS

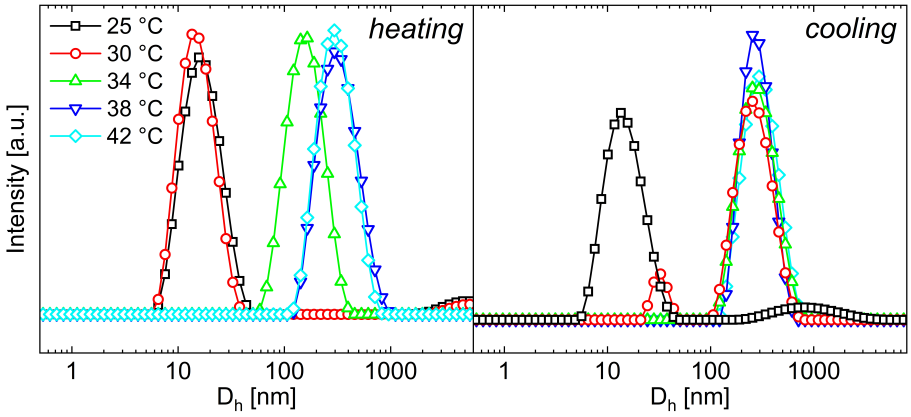

Figure S31: Intensity probability distribution of N_{479}

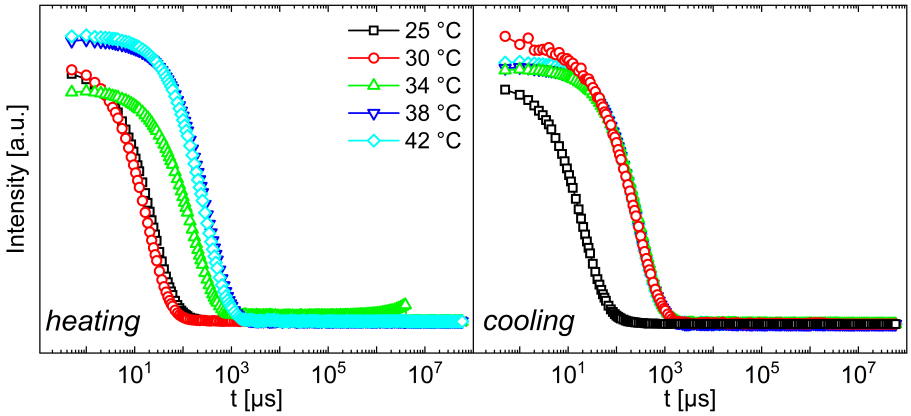

Figure S32: Autocorrelation curves of N_{479}

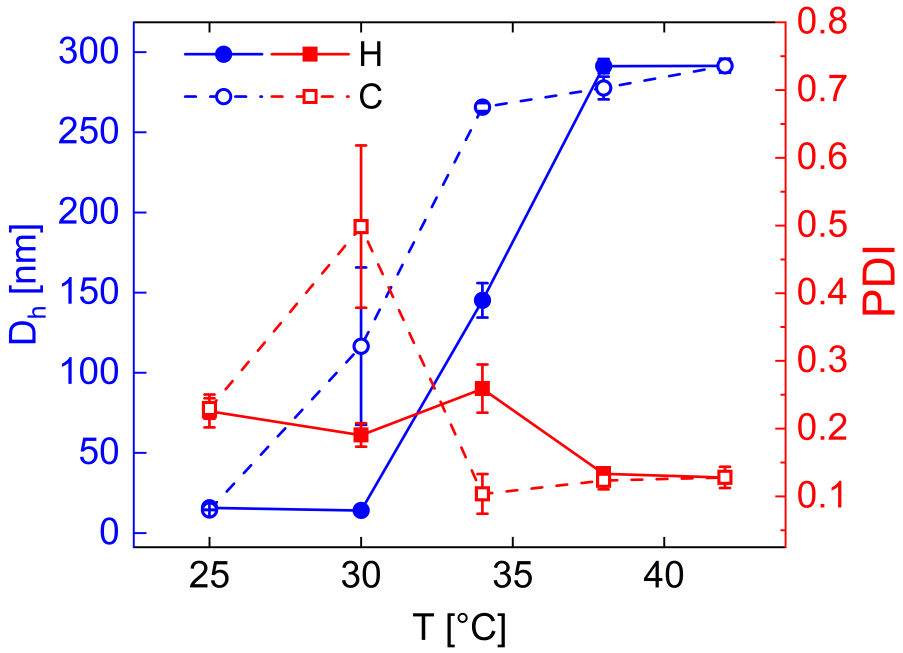

Figure S33: Size and PDI of N_{479} from DLS

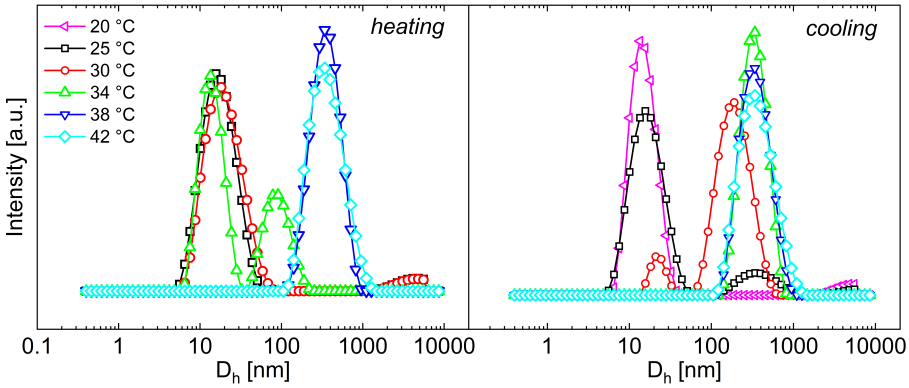

Figure S34: Intensity probability distribution of N_{540}

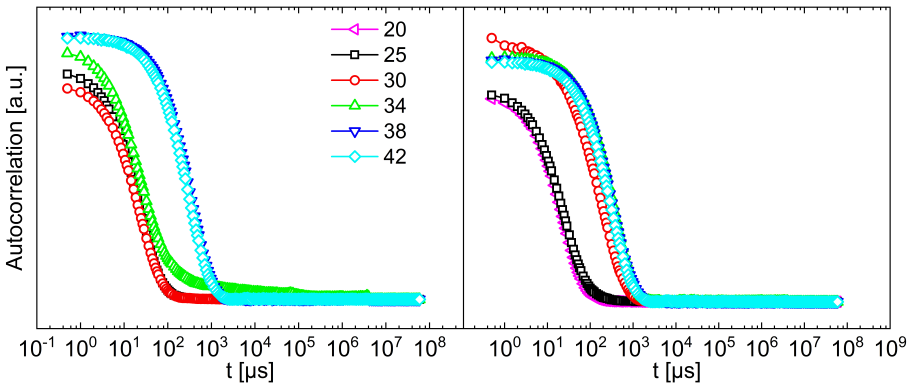

Figure S35: Autocorrelation curves of N_{540}

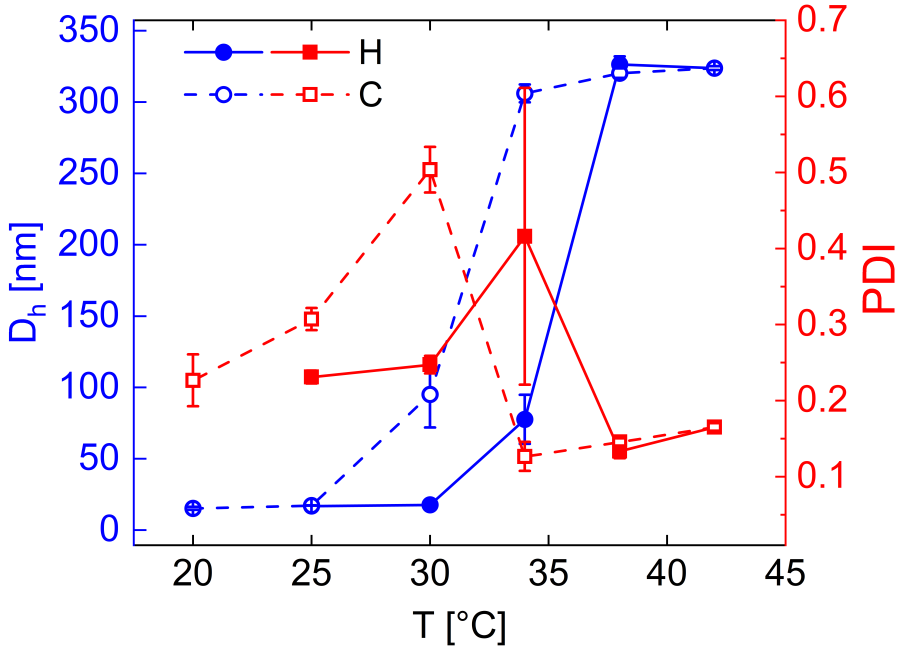

Figure S36: Size and PDI of N_{540} from DLS

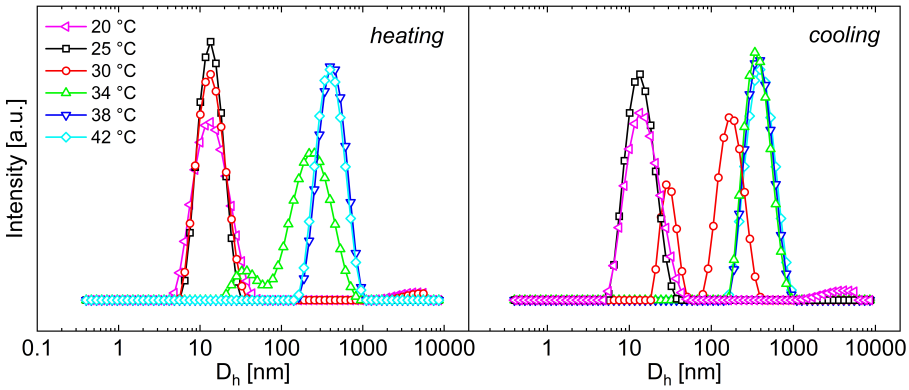

Figure S37: Intensity probability distribution of N_{456}/T_2

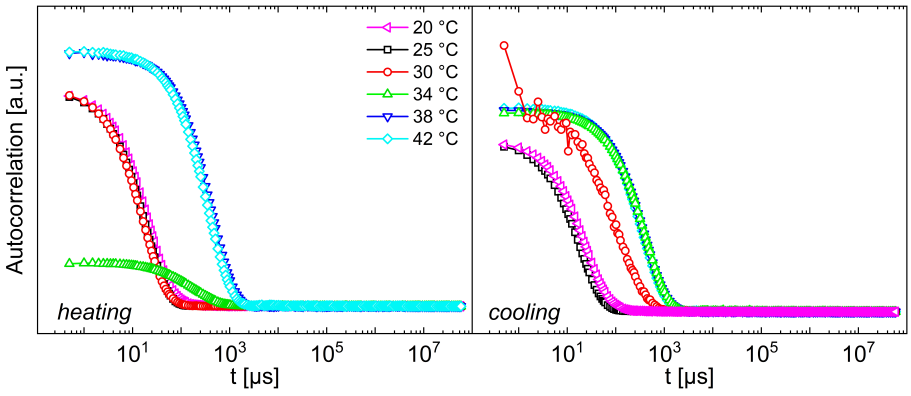

Figure S38: Autocorrelation curves of N_{456}/T_2

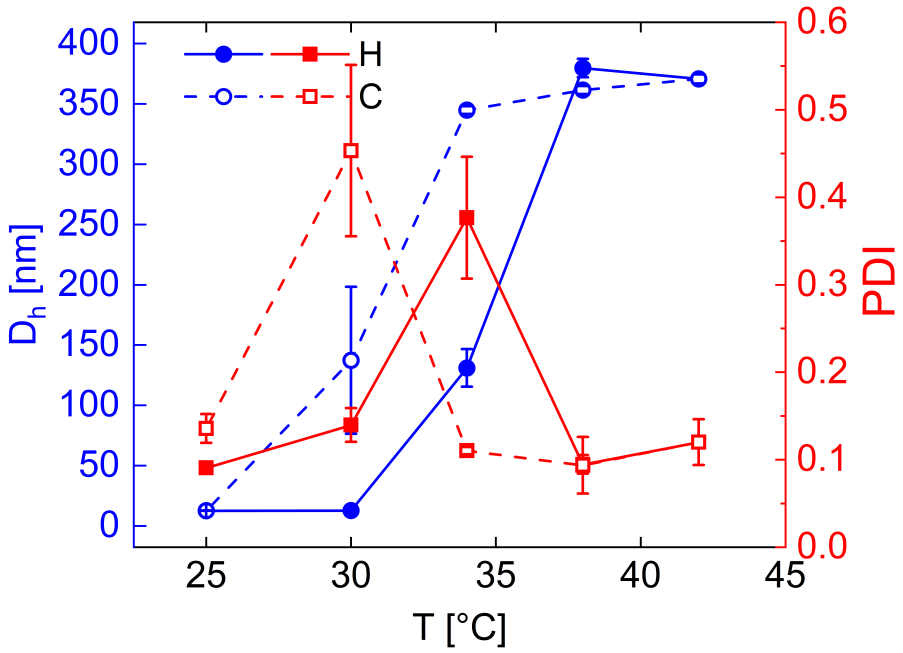

Figure S39: Size and PDI of N_{456}/T_2 from DLS

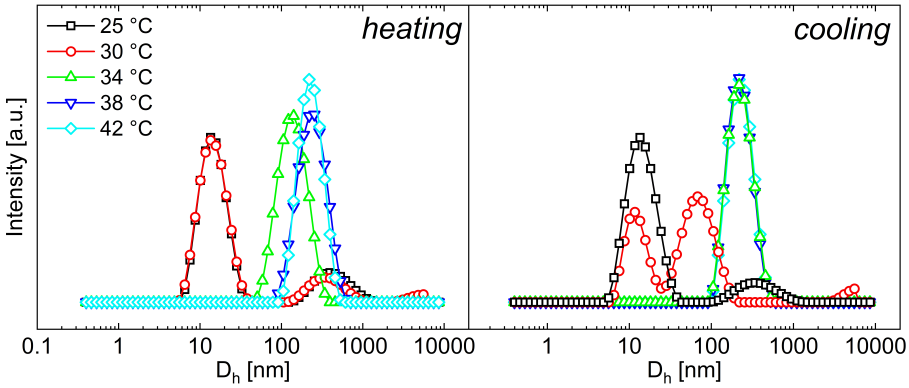

Figure S40: Intensity probability distribution of N_{400}/T_{14}

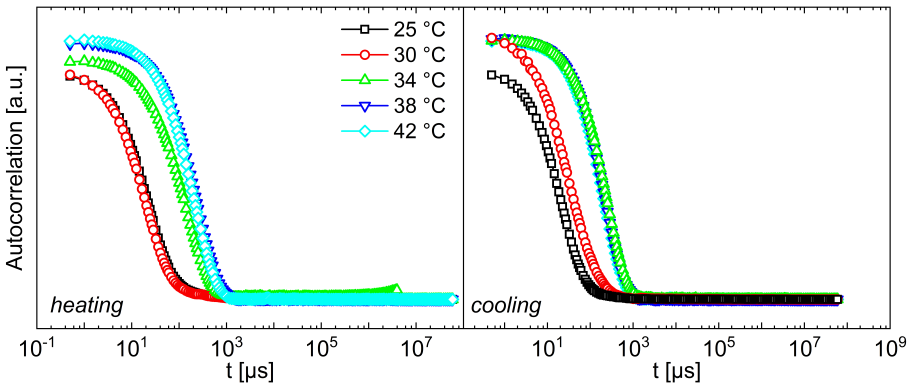

Figure S41: Autocorrelation curves of N_{400}/T_{14}

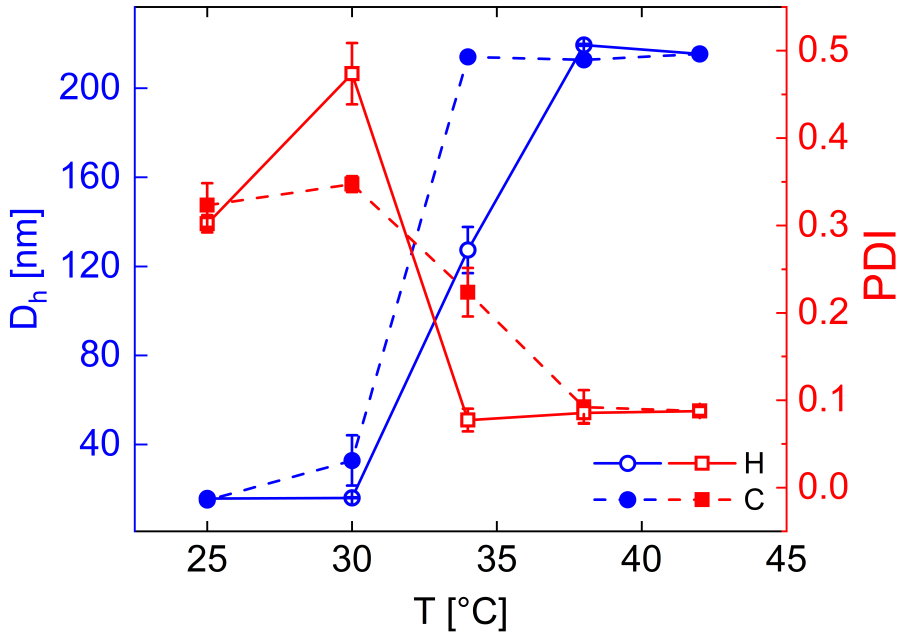

Figure S42: Size and PDI of N_{400}/T_{14} from DLS

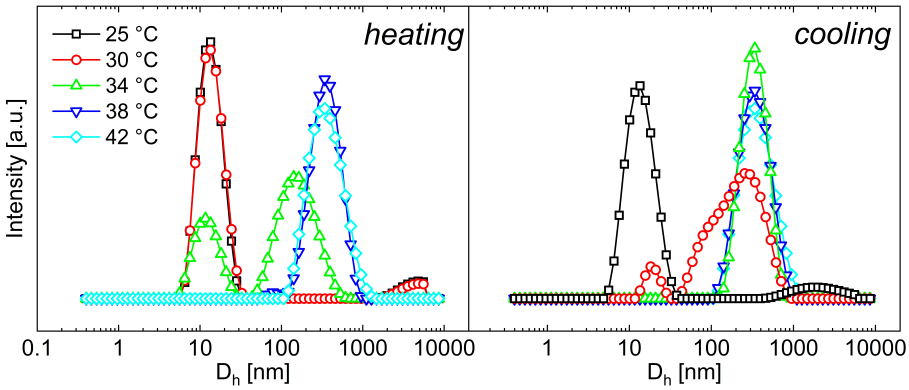

Figure S43: Intensity probability distribution of $N_{337}[N_{88}/T_3]$

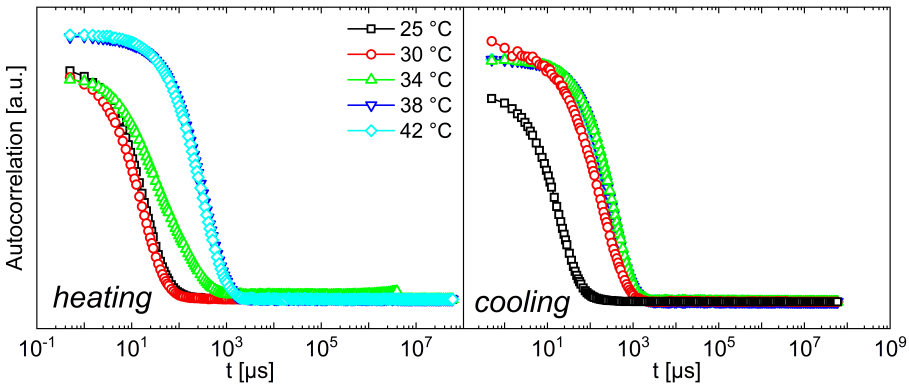

Figure S44: Autocorrelation curves of $N_{337}[N_{88}/T_3]$

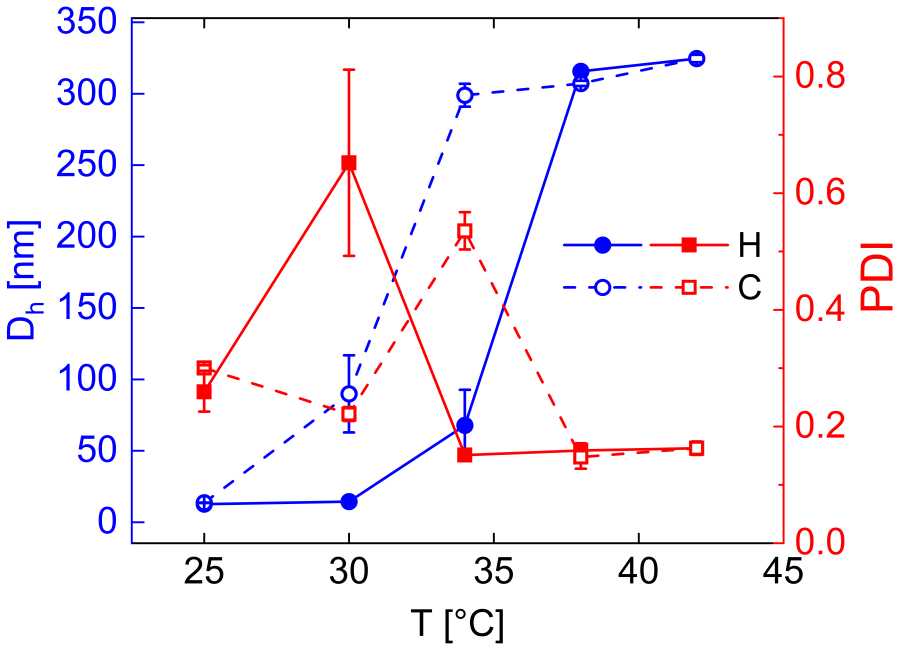

Figure S45: Size and PDI of $N_{337}[N_{88}/T_3]$ from DLS

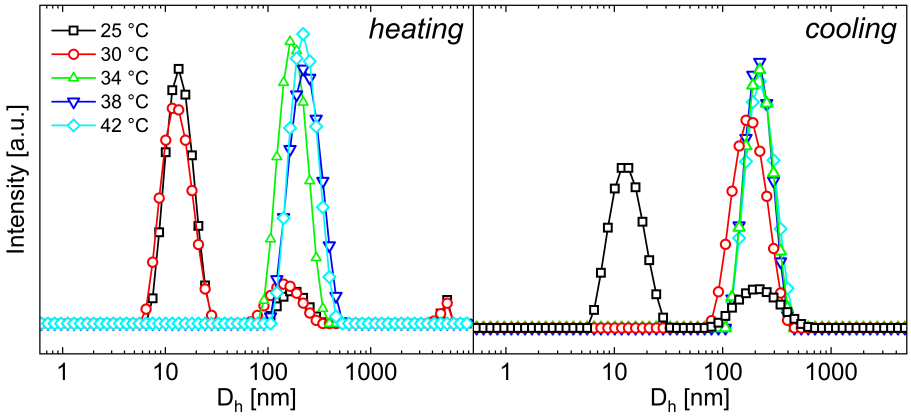

Figure S46: Intensity probability distribution of $N_{363}[N_{113}/T_5]$

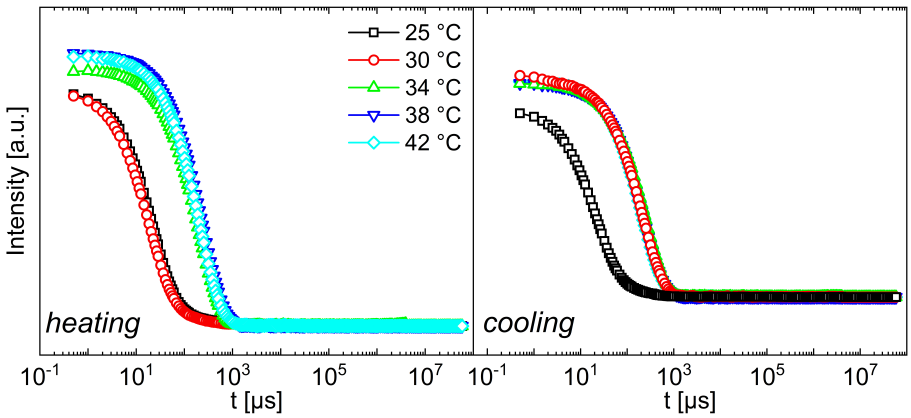

Figure S47: Autocorrelation curves of $N_{363}[N_{113}/T_5]$

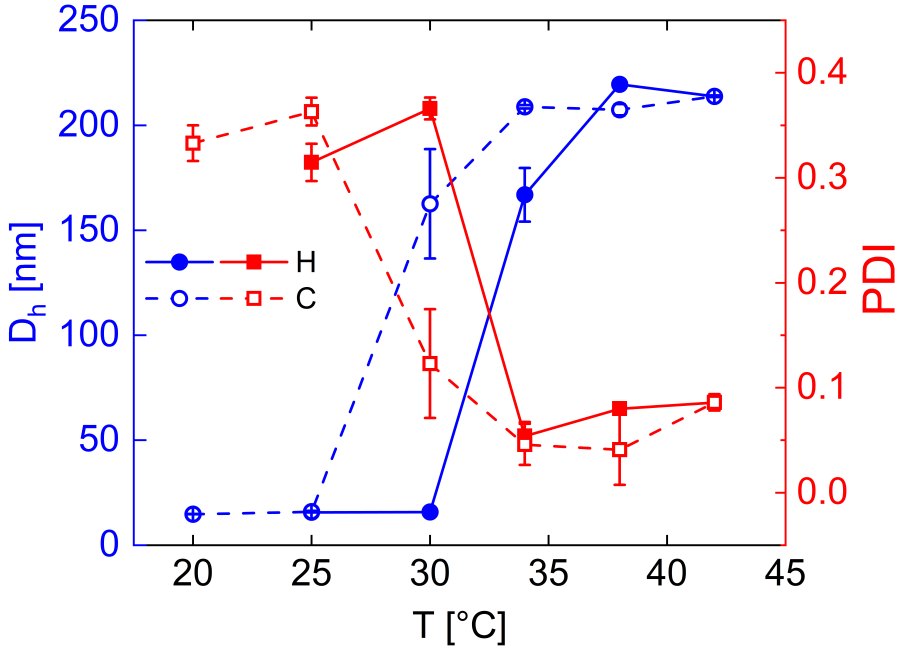

Figure S48: Size and PDI of $N_{363}[N_{113}/T_5]$ from DLS

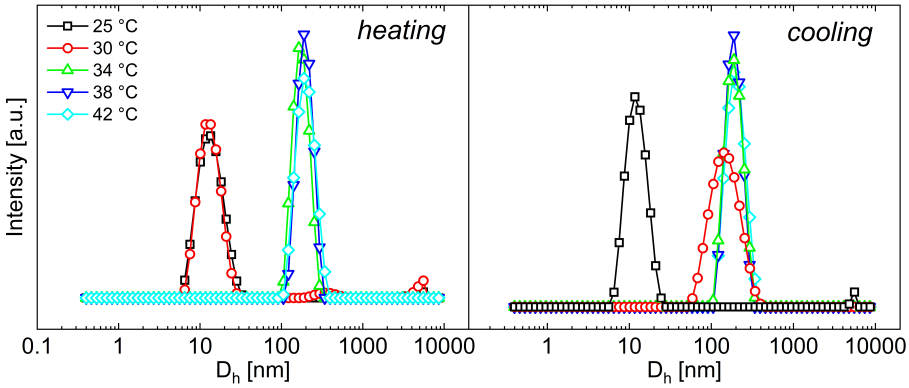

Figure S49: Intensity probability distribution of $N_{293}[N_{143}/T_8]$

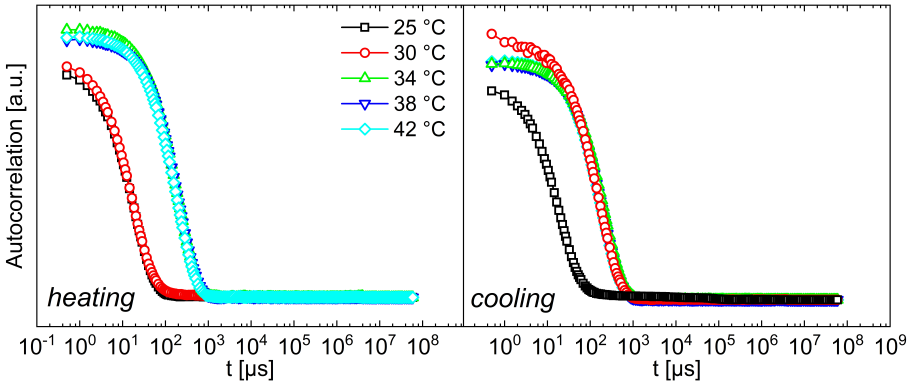

Figure S50: Autocorrelation curves of $N_{293}[N_{143}/T_8]$

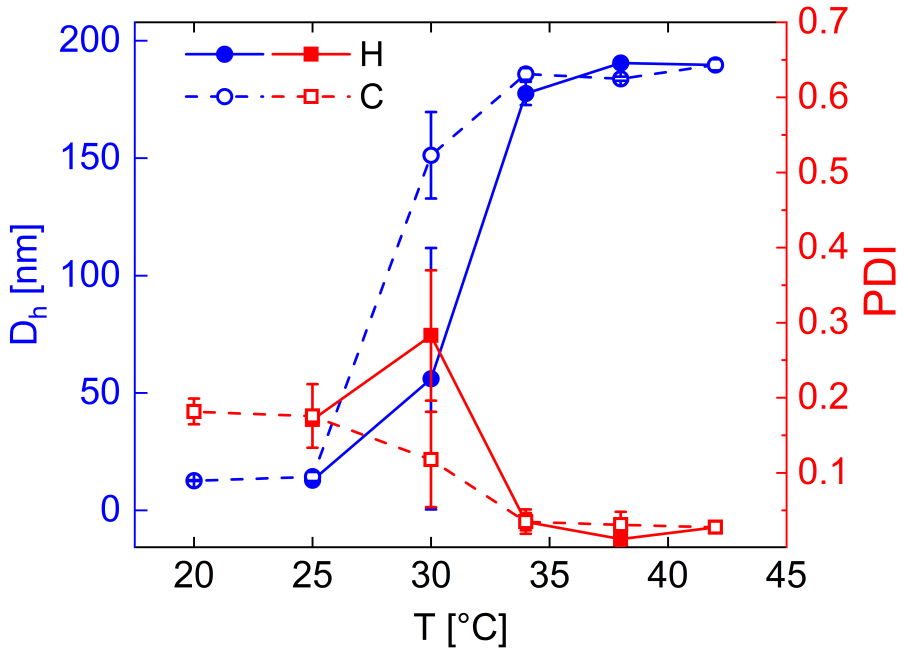

Figure S51: Size and PDI of $N_{293}[N_{143}/T_8]$ from DLS

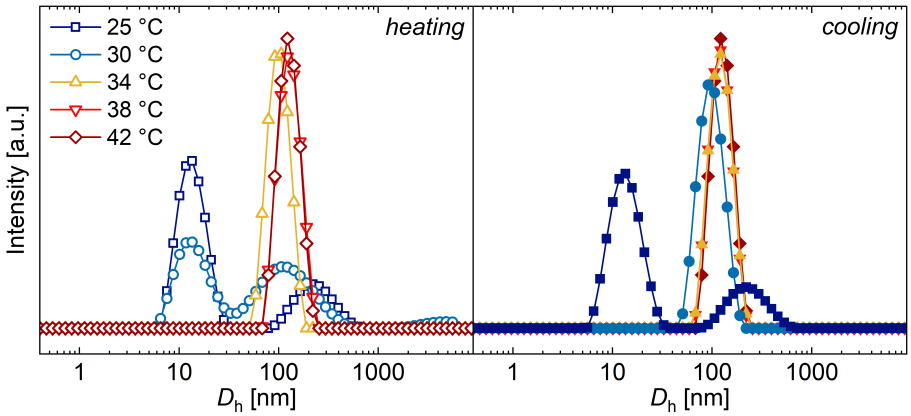

Figure S52: Intensity probability distribution of $N_{283}[N_{113}/T_8]$

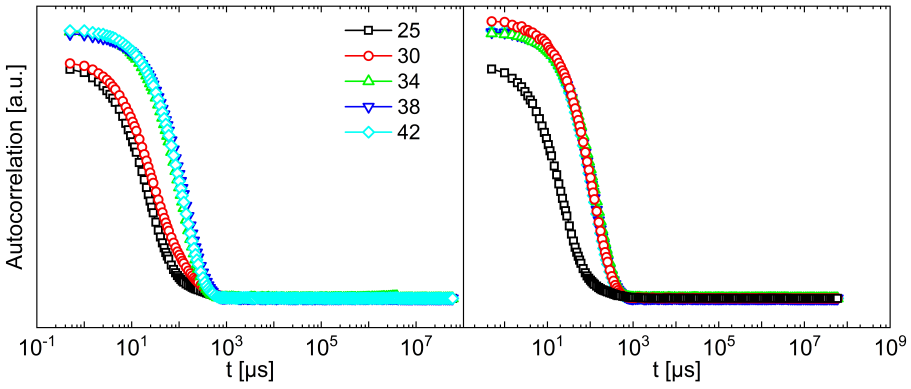

Figure S53: Autocorrelation curves of $N_{283}[N_{113}/T_8]$

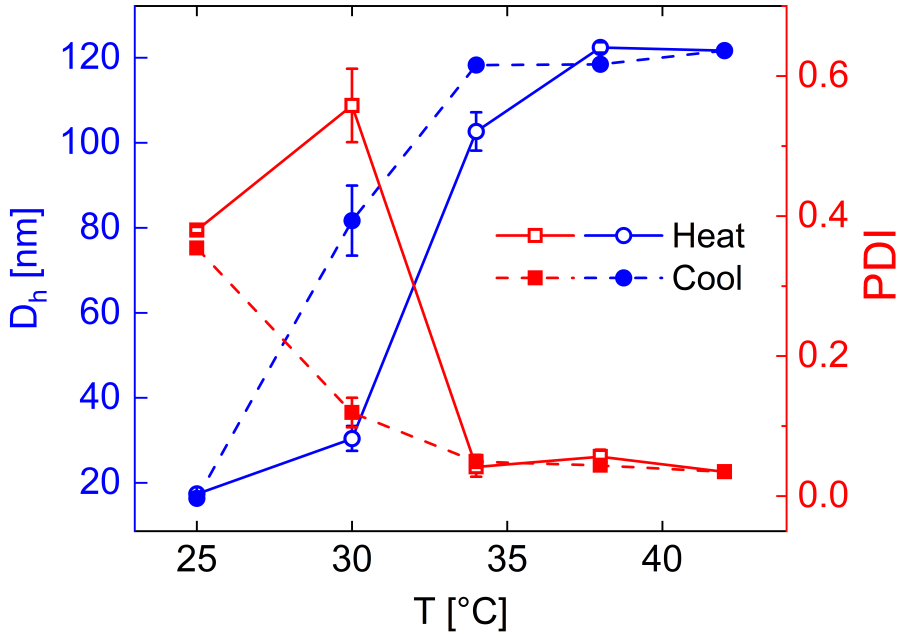

Figure S54: Size and PDI of $N_{283}[N_{113}/T_8]$ from DLS

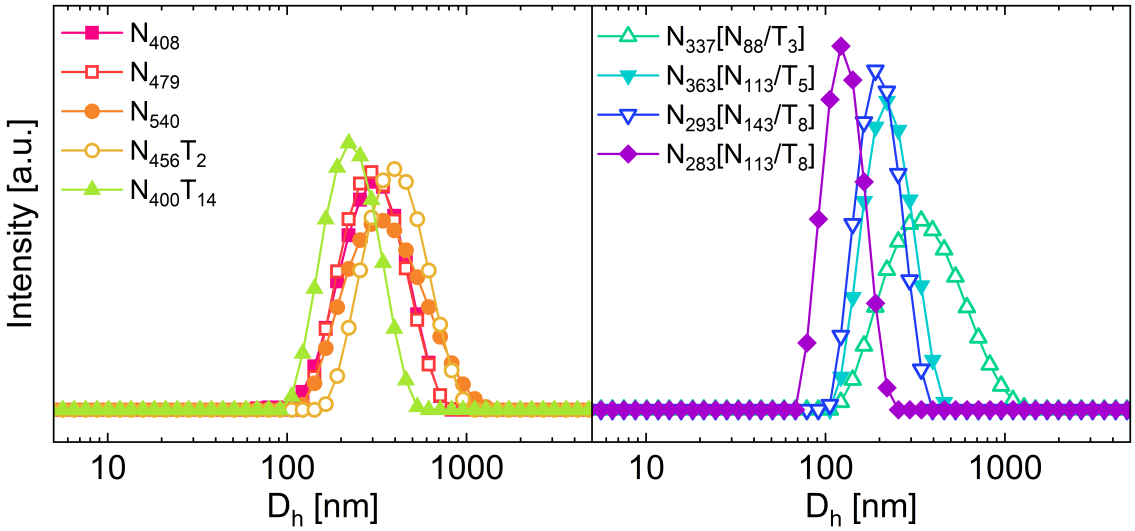

Figure S55: Intensity distributions of D_h at 42 °C for all samples. D_h and PDI decrease with increasing TMA content and localization.

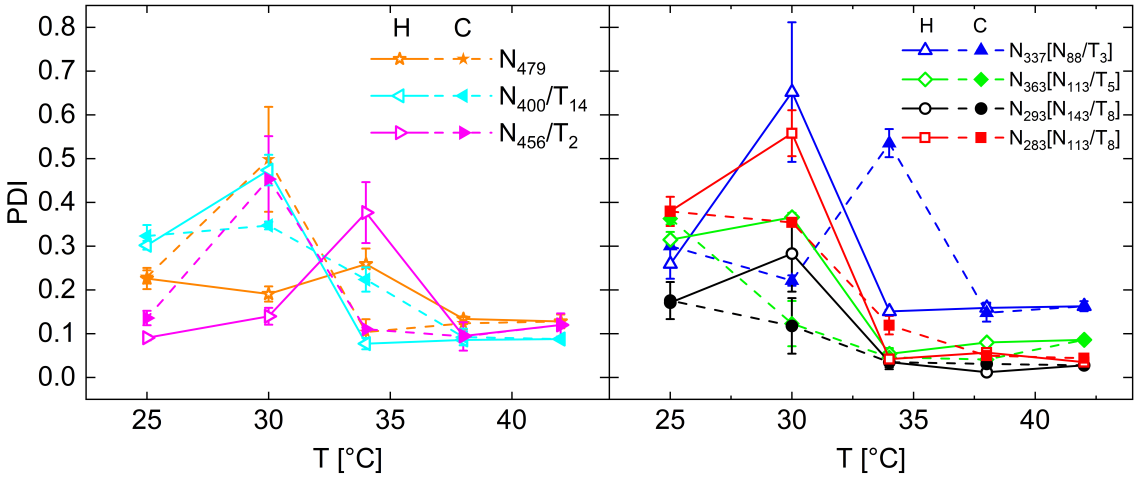

Figure S56: At elevated temperatures blocky functionalized copolymers display small hydrodynamic diameters and PDIs. At high temperatures, error bars are smaller than the points on the graph.

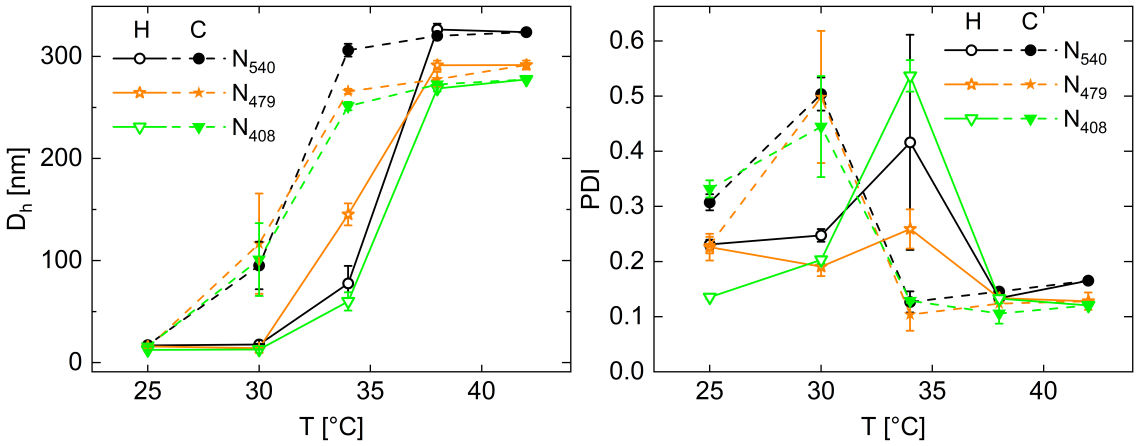

Figure S57: Comparison of homopolymers via DLS

Using JMP statistical software, multivariate analysis was performed between polymer structural parameters and experimental results to help determine the key characteristics controlling the behavior of the systems.

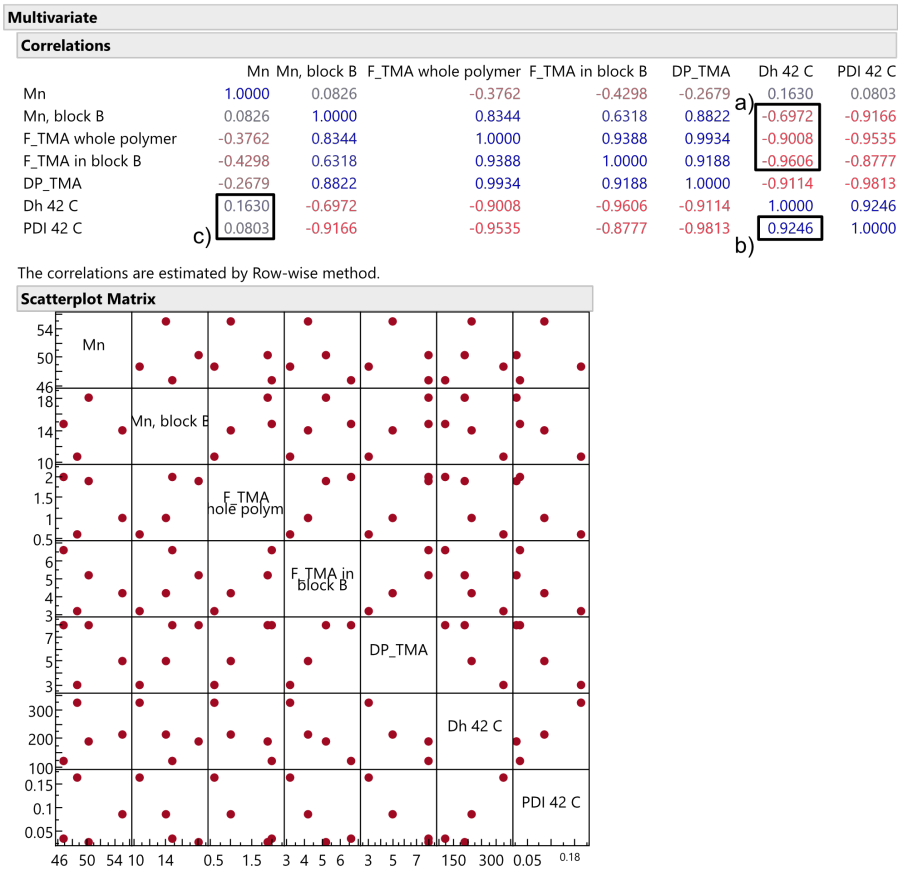

Figure S58: Multivariate analysis of blocky functionalized copolymer structural parameters with DLS size and *PDI*. a) $F_{TMA,B}$ most strongly corresponds to structure size. b) Close correlation between D_h and *PDI* is observed. c) The observed structure size and dispersity is independent of molecular weight

SI.6.1 Concentration effect on DLS for $N_{283}[N_{113}/T_8]$

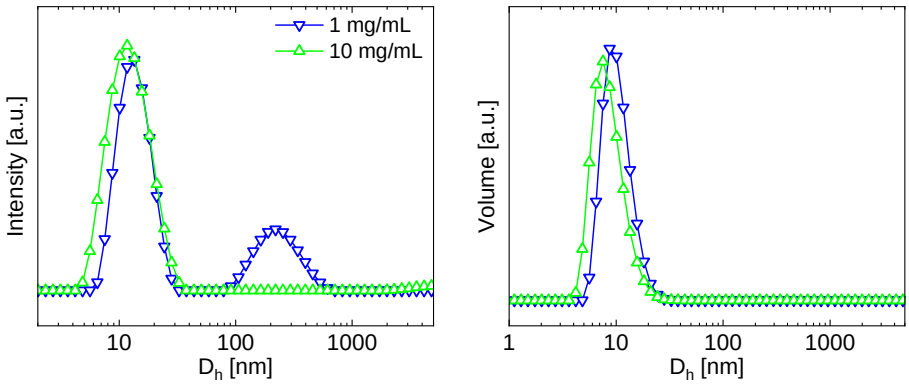

Figure S59: Intensity probability distribution of $N_{283}[N_{113}/T_8]$ at 25°C for 1 mg/mL and 10 mg/mL

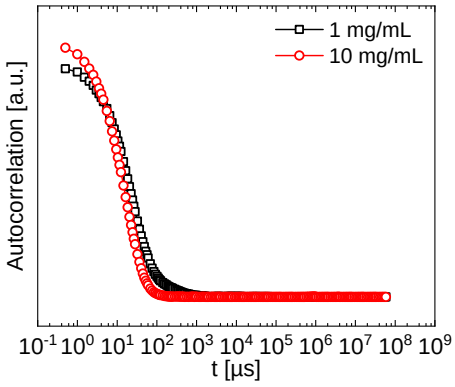

Figure S60: Autocorrelation curves of $N_{283}[N_{113}/T_8]$ at 25°C for 1 mg/mL and 10 mg/mL

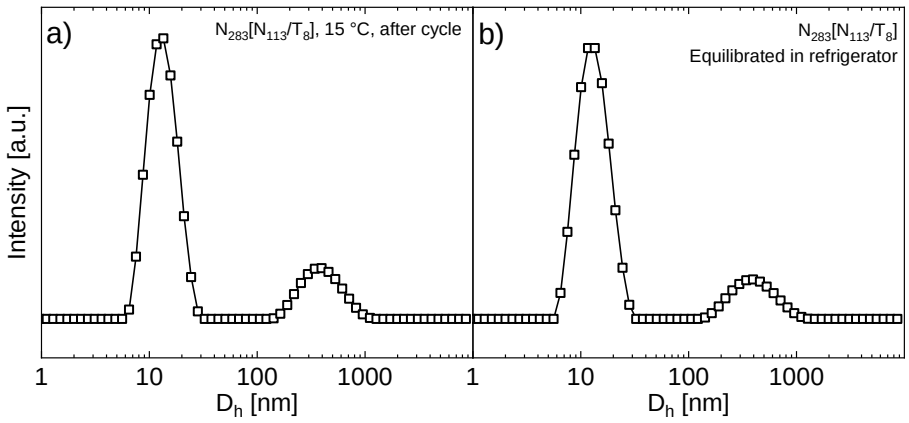

Figure S61: Intensity probability distribution of $N_{283}[N_{113}/T_8]$ (a) at 15°C after DLS temperature ramp and (b) after overnight equilibration in refrigerator at 4 °C (1 mg/mL).

As shown in Fig. S59, DLS measurements at 25 °C show similar unimer size at both 1 mg/mL and 10 mg/mL. Notably, a higher D_h peak appears only in the lower concentration scans. Despite

having a significant contribution to the total scattered intensity, the total volume of this larger population is minimal, as shown in volume distribution shown in Fig. S59. The correlogram (Fig. S61) suggests that these two populations are in coexistence at 1 mg/mL. Given that each of these samples were filtered (0.22 μm PTFE), it is plausible that loose aggregates were filtered out from the 10 mg/mL sample. Low temperature (15°C) scans of $N_{283}[N_{113}/T_8]$ at 1 mg/mL after thermal cycling in the DLS suggest that the higher D_h population persists, and does not substantially change the responsive assembly and aggregation of the polymer.

SI.7 CryoTEM

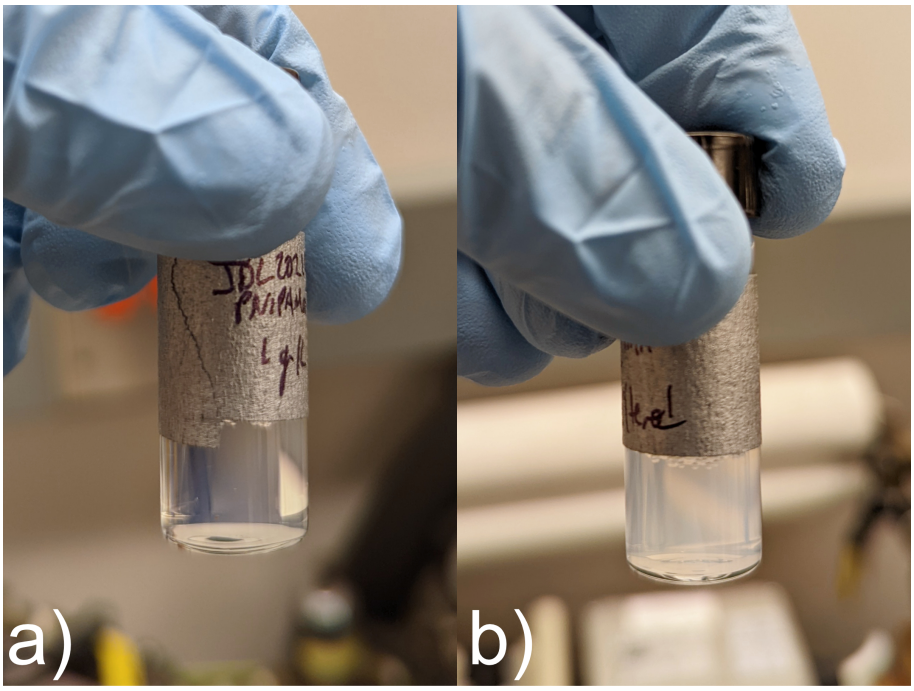

Figure S62: Images of thermally equilibrated samples of a) $N_{283}[N_{113}/T_8]$ and b) N_{456}/T_2 prior to deposition on cryoTEM grids. The blocky functionalized sample appears more translucent with a more pronounced blue hue than the non-blocky copolymer.

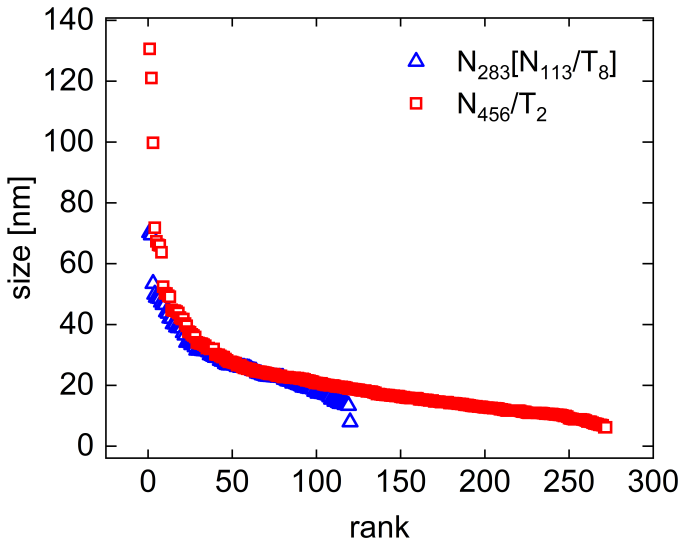

Figure S63: Strutures sized with cryo TEM organized from largest to smallest. Figure of size vs. size rank for N_{456}/T_2 and $N_{283}[N_{113}/T_8]$

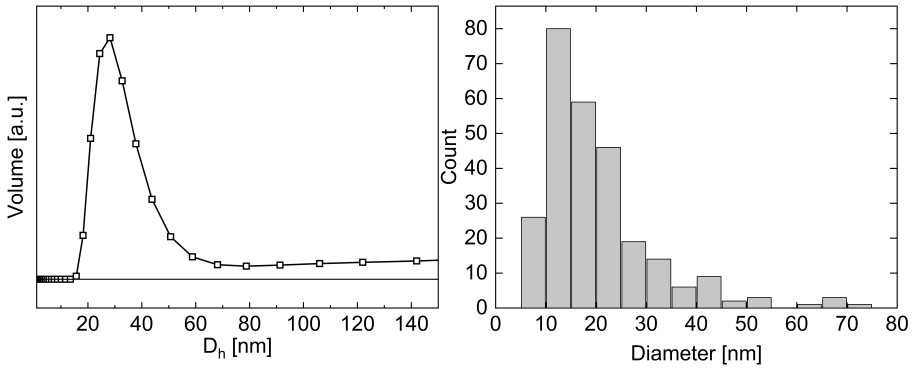

Figure S64: $N_{456}T_2$ transient

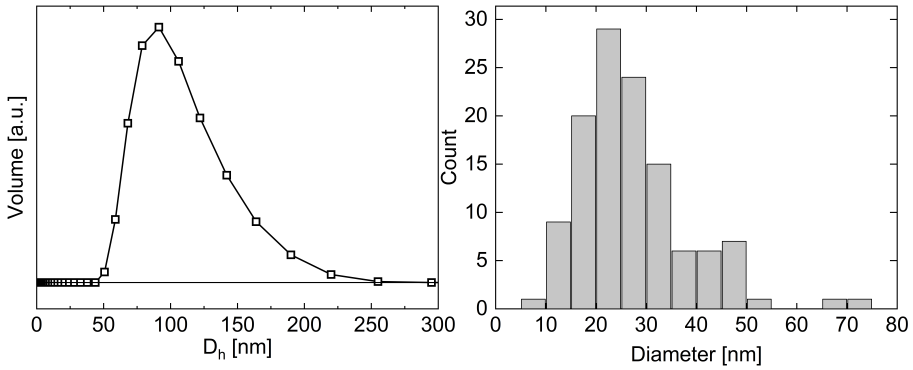

Figure S65: $N_{283}[N_{113}/T_8]$ transient

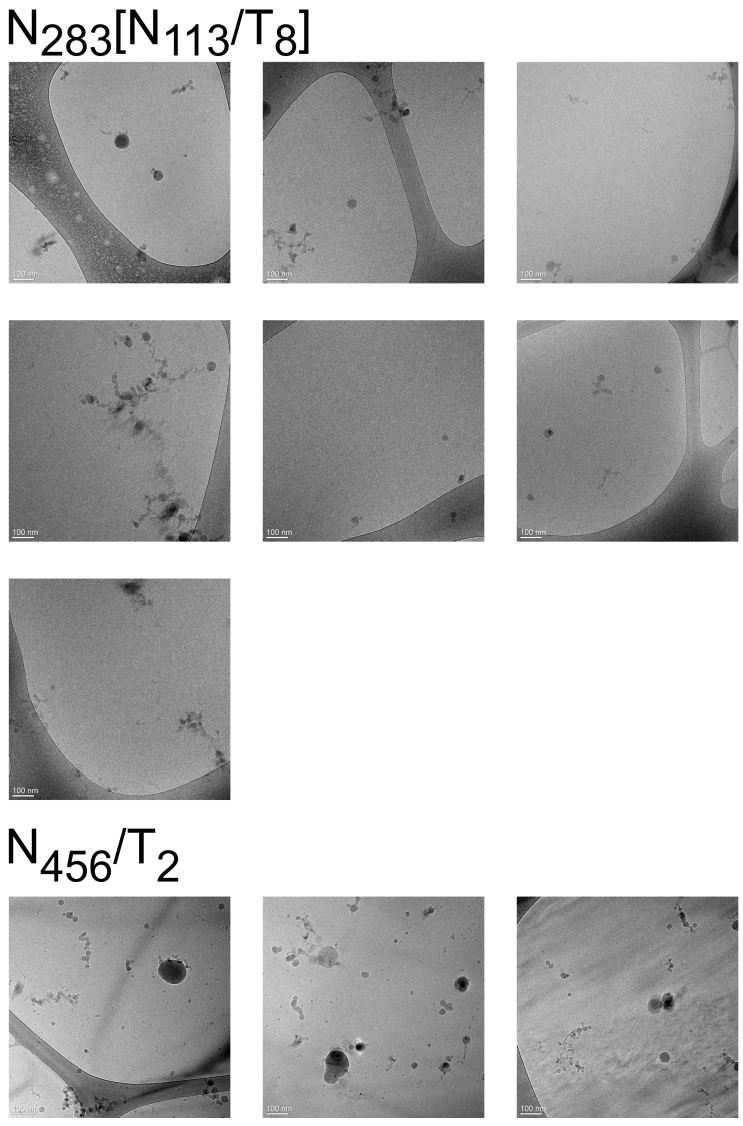

Figure S66: CryoTEM micrographs used for structure sizing for both N_{456}/T_2 and $N_{283}[N_{113}/T_8]$. Due to the areal density of structures, fewer images were used for sizing N_{456}/T_2.

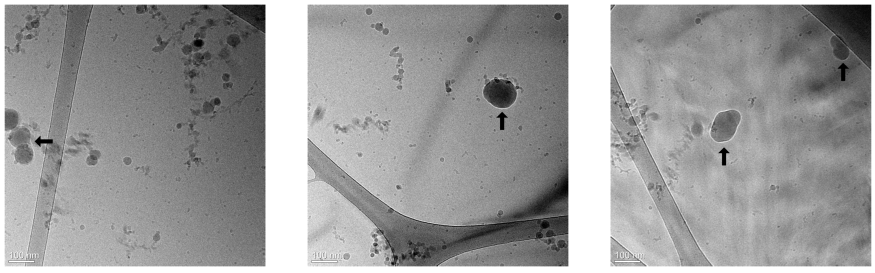

Figure S67: CryoTEM micrographs of N_{456}/T_2 demonstrate large scale fusion events, designated with arrows.

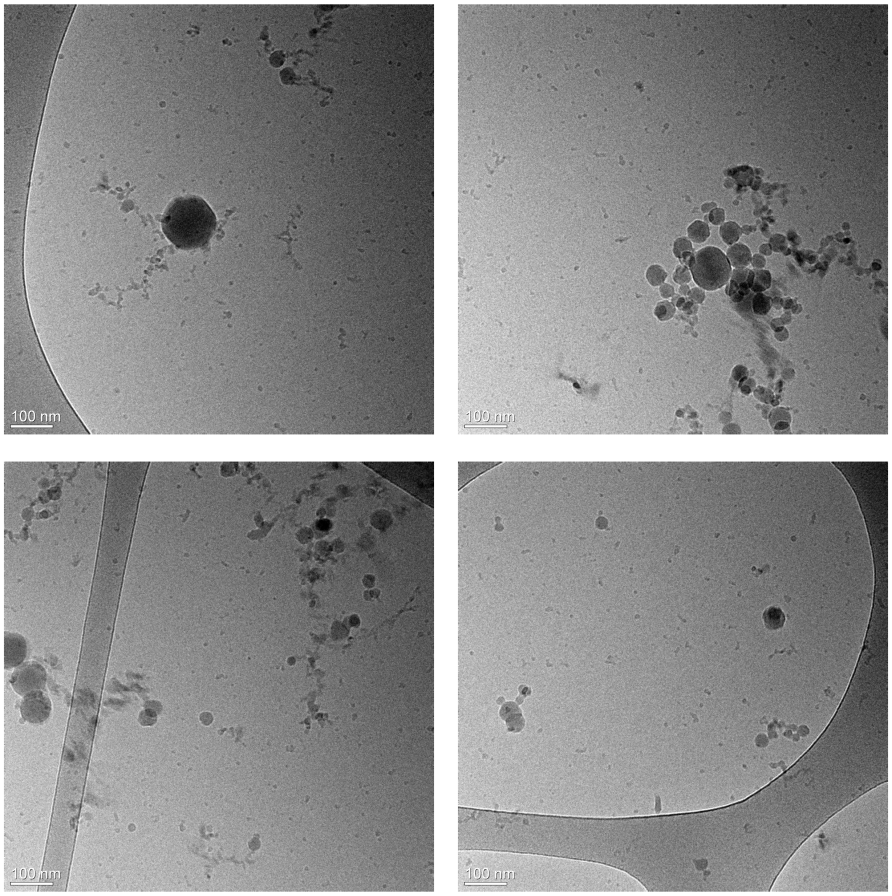

Figure S68: Additional representative cryoTEM micrographs of N_{456}/T_2 *not* used for sizing.

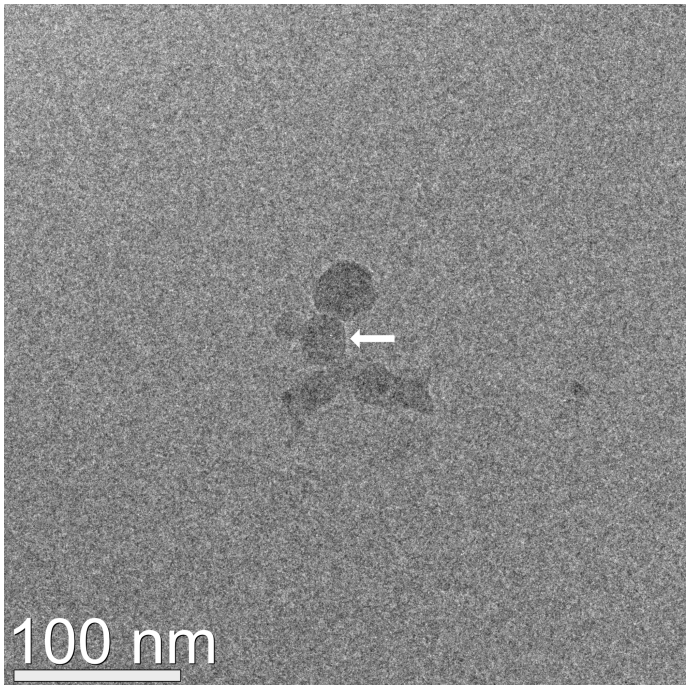

Figure S69: Largest observed merging subunit (marked with arrow) observed in $N_{283}[N_{113}/T_8]$ micrographs has $D_{TEM} = 30.4$ nm

SI.8 Wavelength dependence on P(NIPAM-co-TMA) transmittance

SI.8.1 Ultraviolet-visible (UV-Vis) spectroscopy

UV-vis spectroscopy was used to determine the transmittance of cycled samples over a range of wavelengths. Unlike in homopolymer PNIPAM solutions, solutions of PNIPAM-co-TMA often retain a blue hue after temperature cycling; thus UV-Vis results were used to select the optimal laser wavelength for cloud point testing. Here, a copolymer containing 10% mol TMA was used to prepare 1, 0.5, and 0.1% wt solutions in water. Each sample was cycled four times through a heating and cooling ramp from 20 to 45 °C at a ramp rate of 0.2 °C/min. Fig. S70a&b show the resulting spectrum and a photograph of the room temperature samples after cycling. As shown in Fig. S70a, the samples display similar transmittance values on the CPT using a 650 nm red laser despite visible optical differences (Fig. S70b). As such, a 405 nm laser was used to conduct the vast majority of cloud point testing.

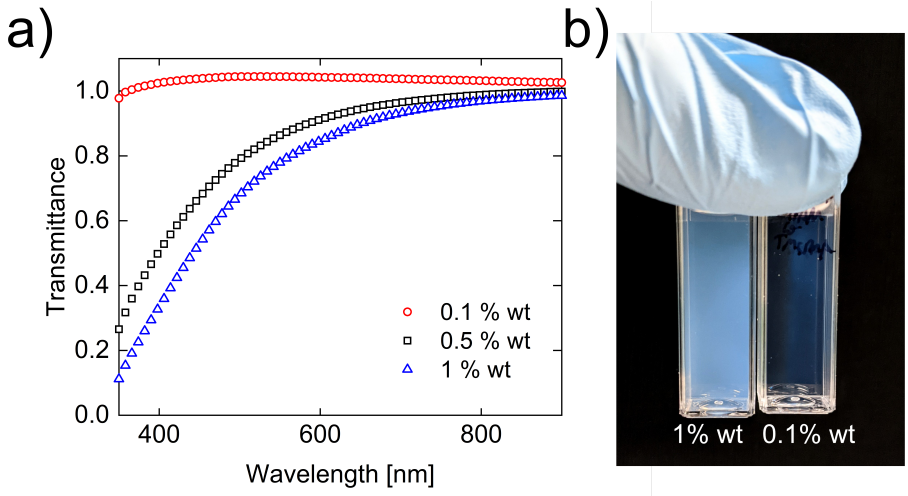

Figure S70: Thermally cycled P(NIPAM-co-TMA) solutions display both a wavelength and concentration dependence. The use of two different lasers in CPT enables the probing of transmittance at multiple wavelengths, giving insight into the type and size of structures formed above T_{CP}.

SI.9 Cloud point testing

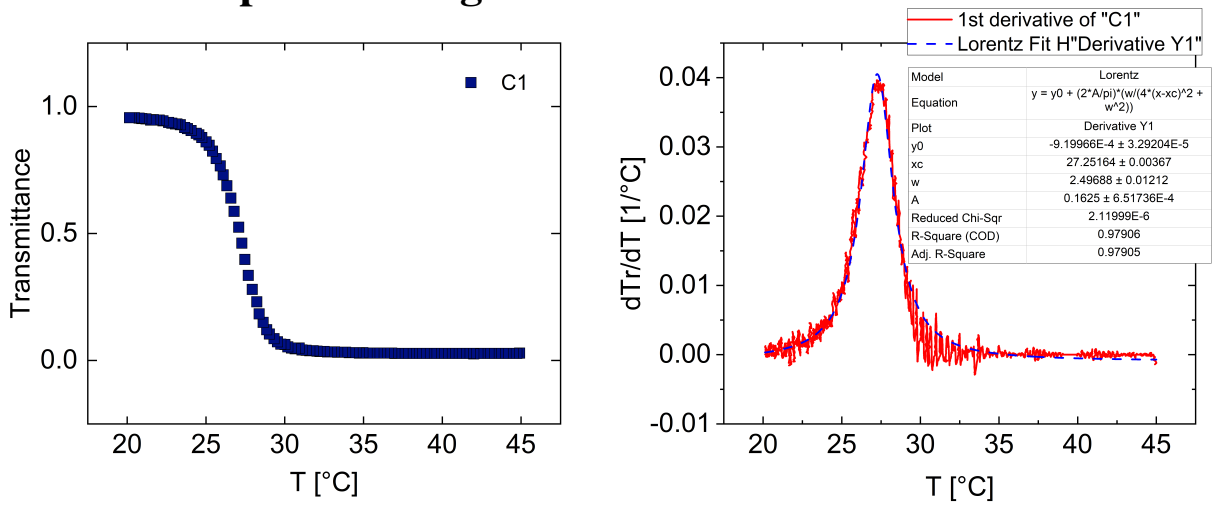

Figure S71: Comparison of transmittance curve and the first derivative of transmittance versus T

Here, T_{CP} and T_{Cl} were calculated using the first derivative of transmission (Tr) with respect to temperature (T). The minimum of $\frac{d\mathrm{Tr}}{dT}$ upon heating and cooling are defined as T_{CP} and T_{Cl}, respectively. Upon cooling, multiple peaks in $\frac{d\mathrm{Tr}}{dT}$ can be observed, which can be attributed to the kinetic processes occurring, including aggregate breakup and reformation of hydrogen bonds between polymer and solvent.[2] T_{Cl} is defined as the minimum in $\frac{d\mathrm{Tr}}{dT}$ at the lowest temperature. When obtaining the derivatives of transmission data, a data smoothing protocol is necessary due to the high polling rate of CPT. Without any smoothing, the derivative is noisy due to the small differences in transmittance between neighboring data points. For these data, a Savitzky-Golay filter is used, where 51 data points are used to fit a 3rd order polynomial, allowing for trends in the derivative to be seen.

SI.10 CPT of PNIPAM homopolymers

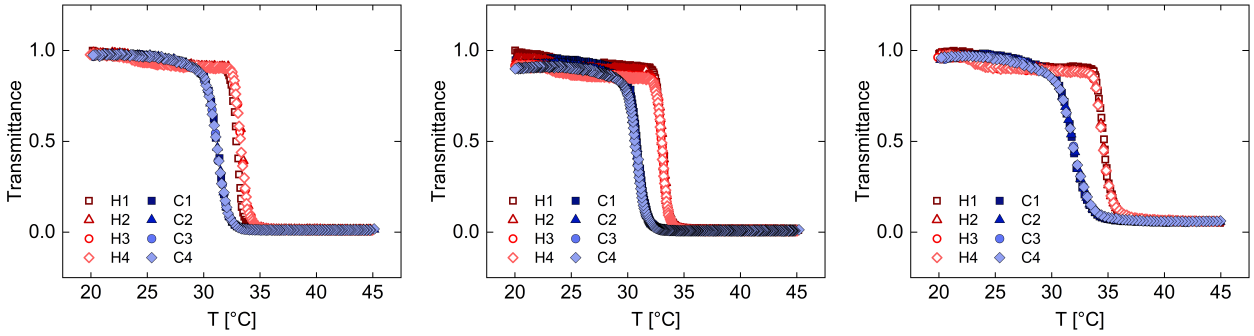

(a) N_{408} (b) N_{479} (c) N_{540}

Figure S72: Transmittance vs. Temperature for three PNIPAM homopolymer controls of DP = 408, 479, 540

SI.11 CPT extracted values

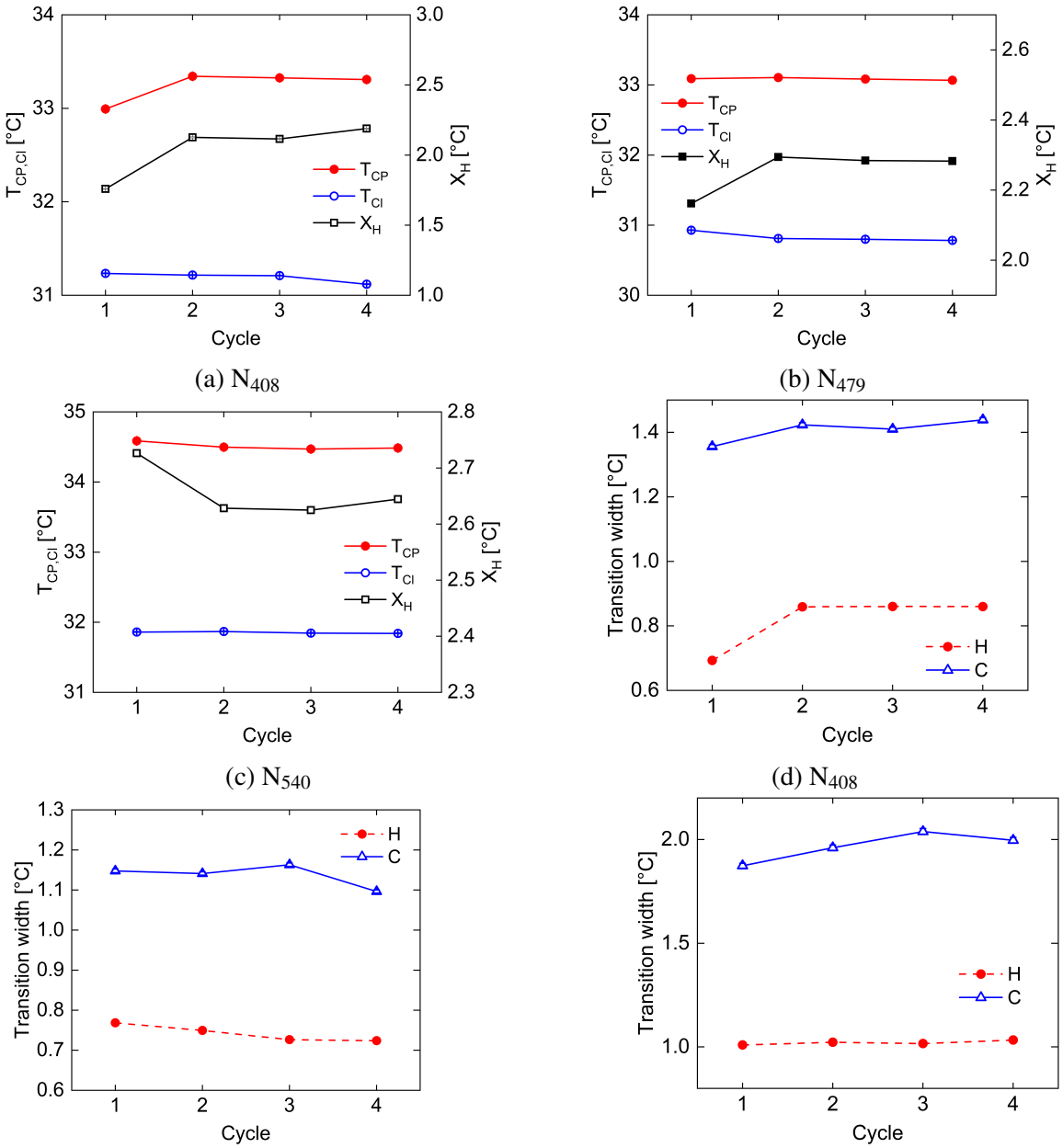

(a) N_{408} (b) N_{479}

(c) N_{540} (d) N_{408}

(e) N_{479} (f) N_{540}

Figure S73: (**a-c**) T_{CP}, T_{Cl}, and X_H values and (**d-f**) w for PNIPAM homopolymer controls of DP = 408, 479, 540

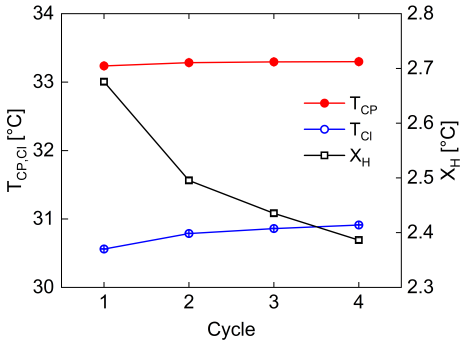

(a) $N_{337}[N_{88}/T_3]$

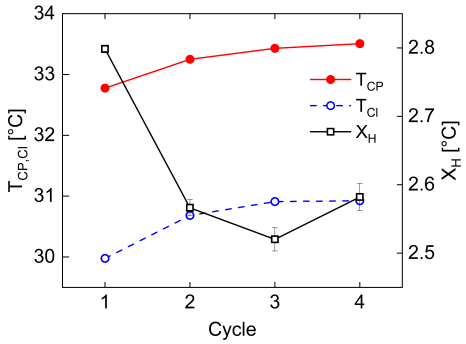

(b) $N_{363}[N_{113}/T_5]$

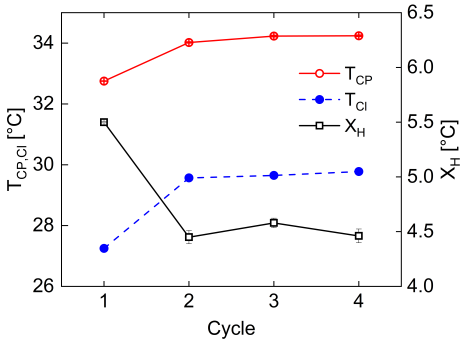

(c) $N_{293}[N_{143}/T_8]$

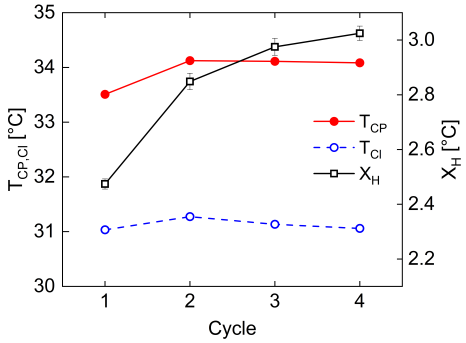

(d) $N_{283}[N_{113}/T_8]$

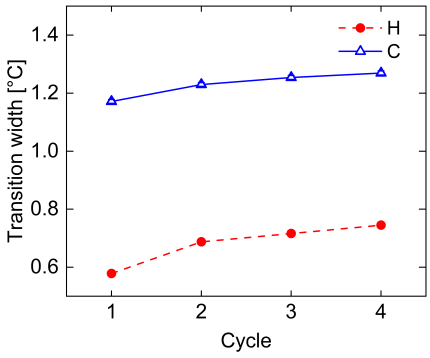

(e) $N_{337}[N_{88}/T_3]$

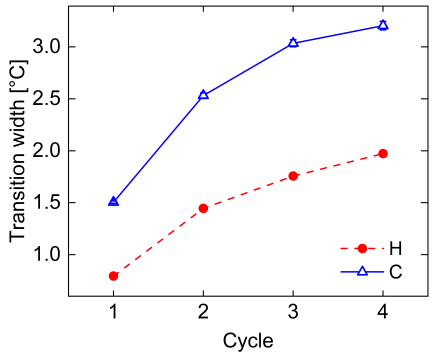

(f) $N_{363}[N_{113}/T_5]$

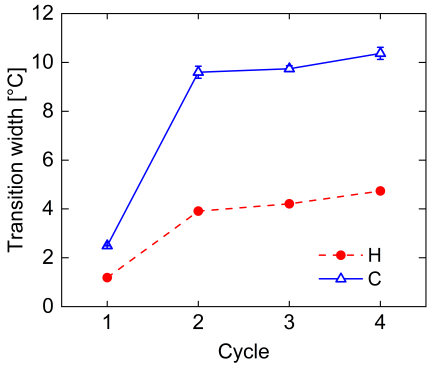

(g) $N_{293}[N_{143}/T_8]$

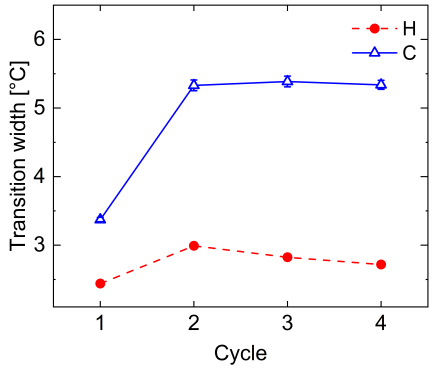

(h) $N_{283}[N_{113}/T_8]$

Figure S74: (**a-c**) T_{CP}, T_{Cl}, and X_H values and (**d-f**) w for AB blocky functionalized PNIPAM-co-TMA copolymers

SI.12 CPT results with red laser

CPT results with the red laser qualitatively agree with results using the violet laser across samples. In high TMA-containing blocky-functionalized copolymers, the same qualitative behavior and reduced ΔTr is observed upon repeated cycling; however now, the transmittance drop is minimal with increasing cycle numbers. This finding is consistent with the formation of semi-permanent smaller-scale structures due to silane coupling, as the scattering from smaller structures is not well-suited for the red laser.

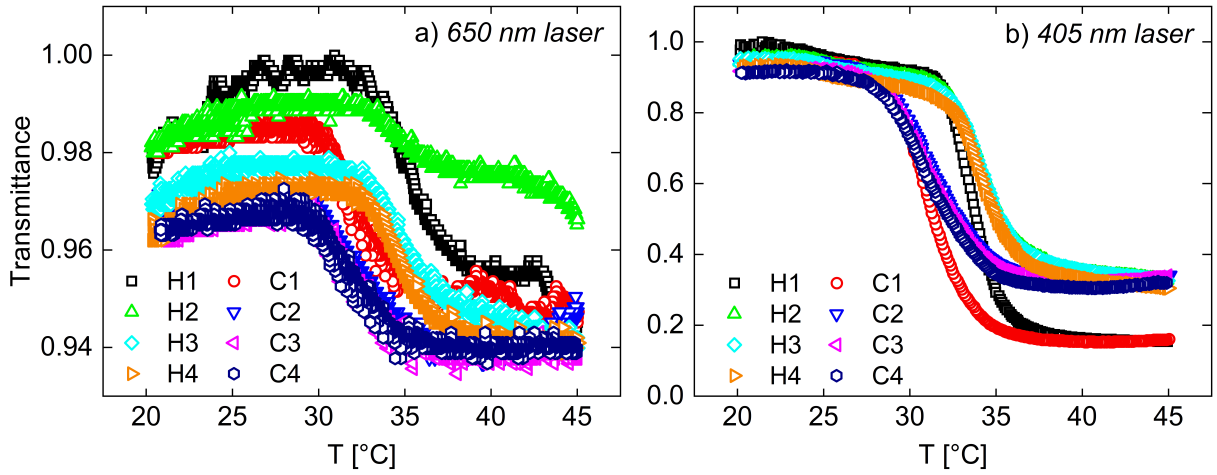

Figure S75: CPT using two different lasers yields substantial differences in the signal quality, indicating that the samples have greater transmittance at high wavelengths for $N_{283}[N_{113}/T_8]$

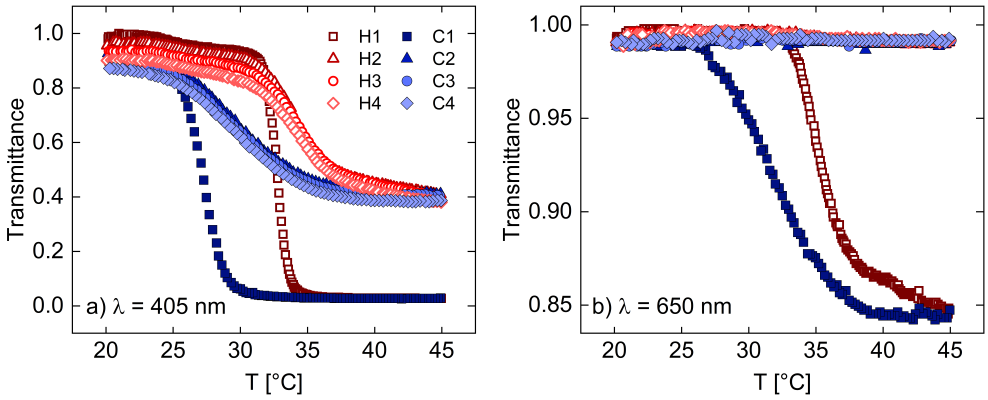

Figure S76: Transmittance response of $N_{293}[N_{143}/T_8]$ with thermal cycling with two different laser wavelengths.

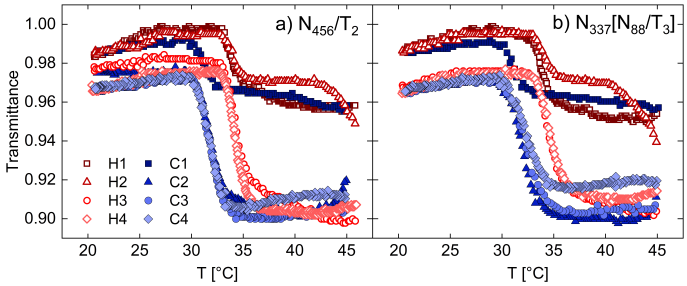

Figure S77: N_{456}/T_2 (a) and $N_{337}[N_{88}/T_3]$ (b) display similar trends in CPT performed with a red laser ($\lambda = 650$ nm), with the transmittance drop on repeated cycling likely due to inter-chain coupling

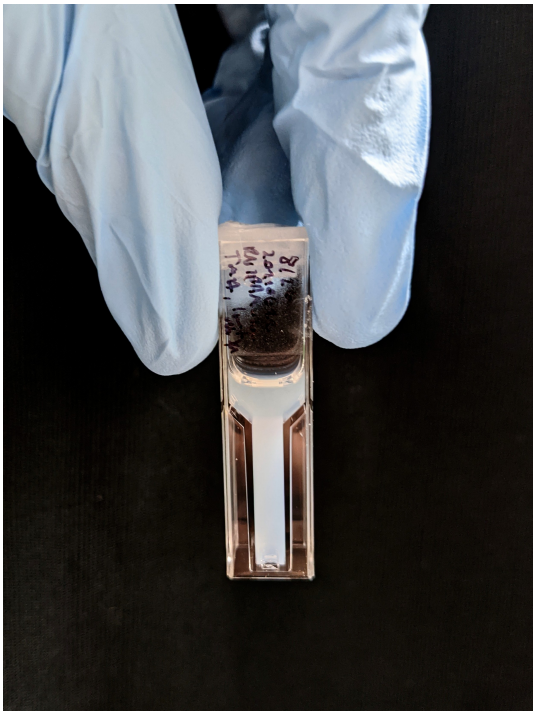

Figure S78: N_{400}/T_{14} after thermal cycling via CPT

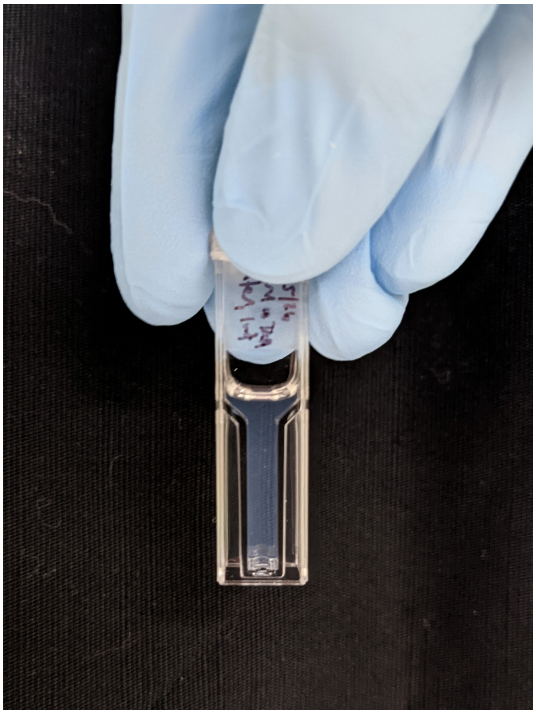

Figure S79: $N_{293}[N_{143}/T_8]$ after thermal cycling via CPT

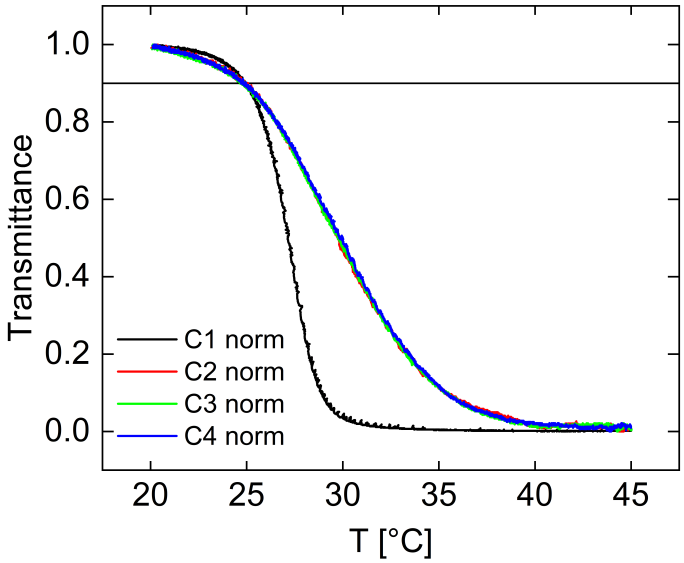

Figure S80: Transmittance vs. T $N_{293}[N_{143}/T_8]$ upon cooling show similar temperature at 90% transmittance, regardless of cycle when each temperature ramp is normalized

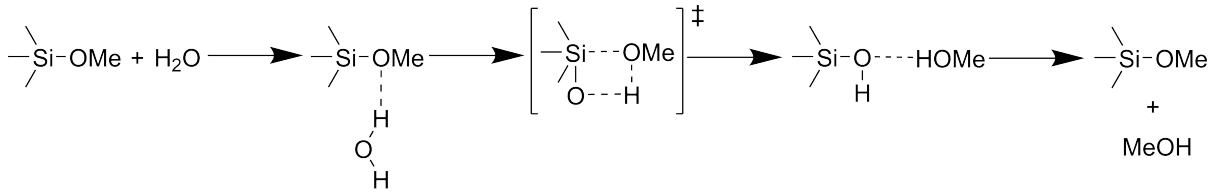

Figure S81: Mechanism of methoxysilane hydrolysis under neutral conditions. Figure modified from Issa and Luyt.[4]

SI.13 Variable temperature NMR

Due to differences between the sample temperature and the instrument set temperature, calibration curves were created using an ethylene glycol standard and a built-in macro to find the sample temperature. The relationship between the set and sample temperature was found to be consistent across multiple days. In the relevant temperature range of approximately 20 to 45 °C, a linear trend was found between the calibrated and set temperatures, as show in Fig. S82a.

A second calibration was created using the difference in chemical shifts between the D_2O solvent peak in the polymer samples and the DSS. The chemical shifts of D_2O and DSS change with temperature, as reported in the literature.[3] Fig. S82 shows the chemical shift of D_2O (where DSS is referenced to 0 ppm) vs. temperature. The data points were calibrated from the ethylene glycol standard with the fit shown in red. The literature fit from Hoffman is shown in blue. For consistency, the fit shown in red is used to calculate the sample temperature based on the solvent peak in the variable temperature spectra. This procedure reduces the need to construct a calibration curve prior to each experimentation because the temperature can be calculated directly from the experimental sample.

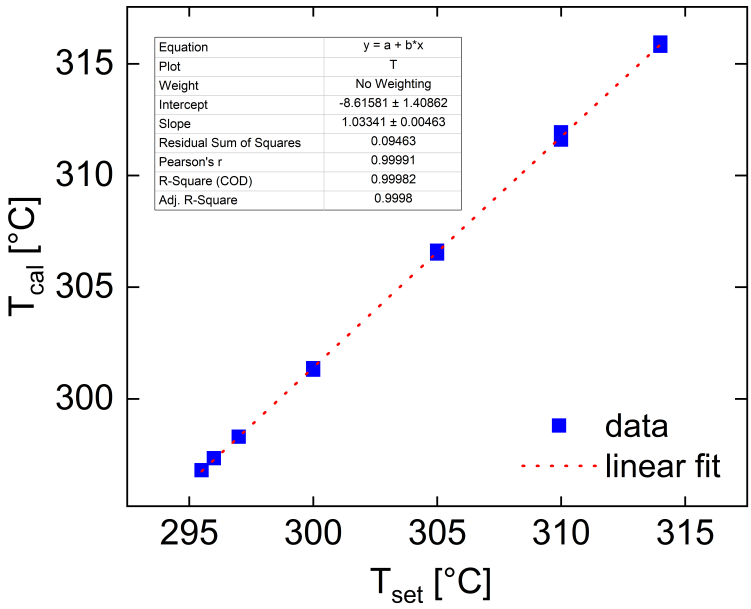

(a) Calibrated temperature vs. set temperature as determined by an ethylene glycol standard with a built-in macro

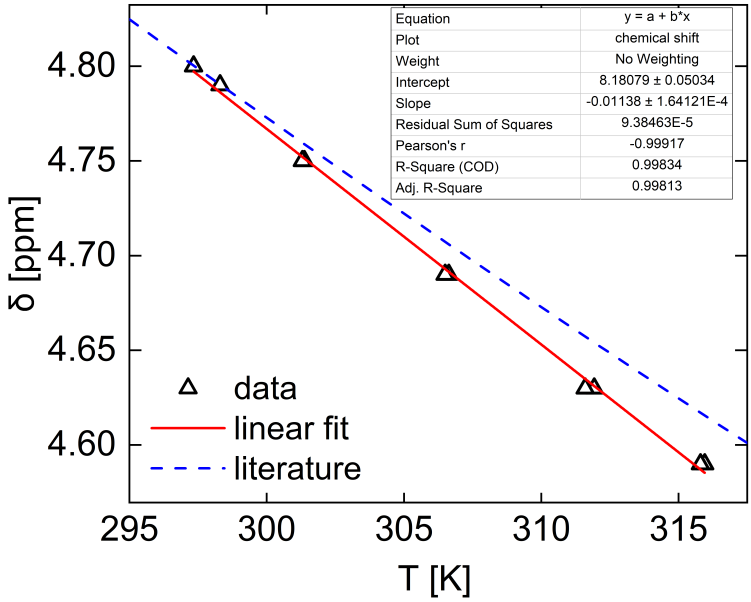

(b) Calibration curve constructed using the difference in chemical shift between D_2O and DSS vs. calibrated temperature

Figure S82: Temperature calibrations used for VT NMR experiments

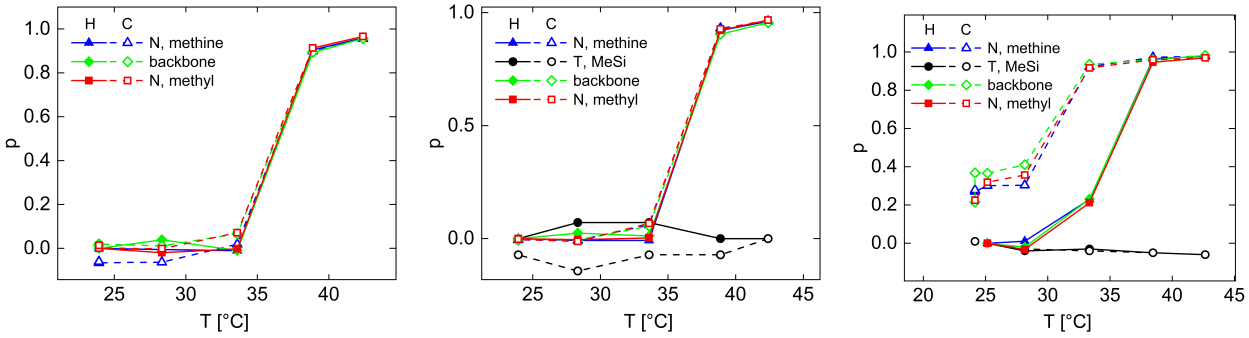

(a) N_{408} (b) $[N_{456}/T_2]$ (c) $[N_{400}/T_{14}]$

Figure S83: p vs. temperature for non-blocky PNIPAM and PNIPAM-co-TMA shows that hysteresis and permanent immobilization largely depends on the TMA content

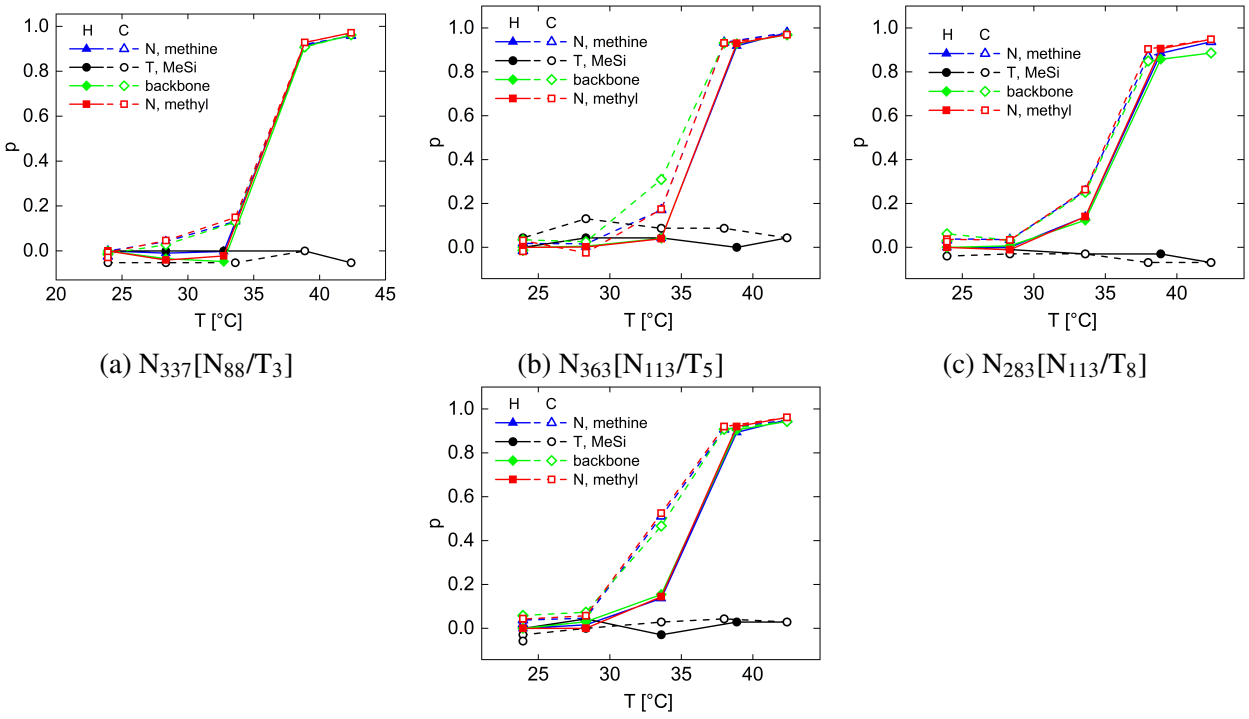

(a) $N_{337}[N_{88}/T_3]$ (b) $N_{363}[N_{113}/T_5]$ (c) $N_{283}[N_{113}/T_8]$

(d) $N_{293}[N_{143}/T_8]$

Figure S84: p vs. temperature for blocky PNIPAM-co-TMA shows that hysteresis behavior not seen in the PNIPAM homopolymer while achieving nearly full recovery of p.

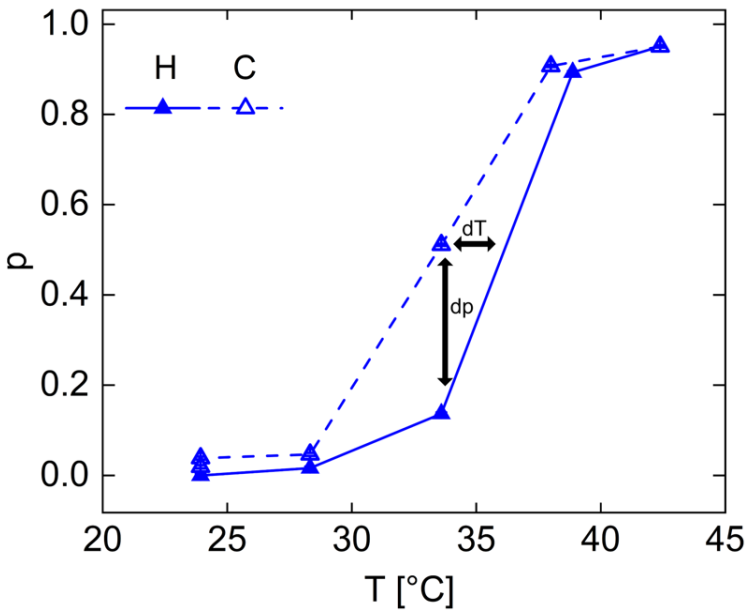

Figure S85: Three parameters were used to quantify the hysteresis in VT NMR experiment. (1) the difference in p at 34 °C between heating and cooling (dP_{34C}), (2) the difference in T at $p = 0.5$ between heating and cooling ($dT_{p=0.5}$), and (3) the difference in p before and cycling at low T (dP_{cycle}). The dT at 34 °was calculated using a linear construction between points. Hysteresis calculations were performed using the data corresponding to the protons labelled **A** in Fig. 11

Multivariate

Correlations

	Mn	Mn, block A	Mn, block B	F_TMA whole polymer	F_TMA in block B	dP, 34C	dT, p=0.5	dP, cycle
Mn	1.0000	0.7321	0.0826	-0.3762	-0.4298	0.0416	0.1401	-0.5163
Mn, block A	0.7321	1.0000	-0.6184	-0.8671	-0.7708	-0.5020	-0.5451	-0.9009
Mn, block B	0.0826	-0.6184	1.0000	0.8344	0.6318	0.7823	0.9590	0.7223
F_TMA whole polymer	-0.3762	-0.8671	0.8344	1.0000	0.9388	0.4621	0.6836	0.9835
F_TMA in block B	-0.4298	-0.7708	0.6318	0.9388	1.0000	0.1284	0.4088	0.9659
dP, 34C	0.0416	-0.5020	0.7823	0.4621	0.1284	1.0000	0.9210	0.3421
dT, p=0.5	0.1401	-0.5451	0.9590	0.6836	0.4088	0.9210	1.0000	0.5524
dP, cycle	-0.5163	-0.9009	0.7223	0.9835	0.9659	0.3421	0.5524	1.0000

The correlations are estimated by Row-wise method.

Scatterplot Matrix

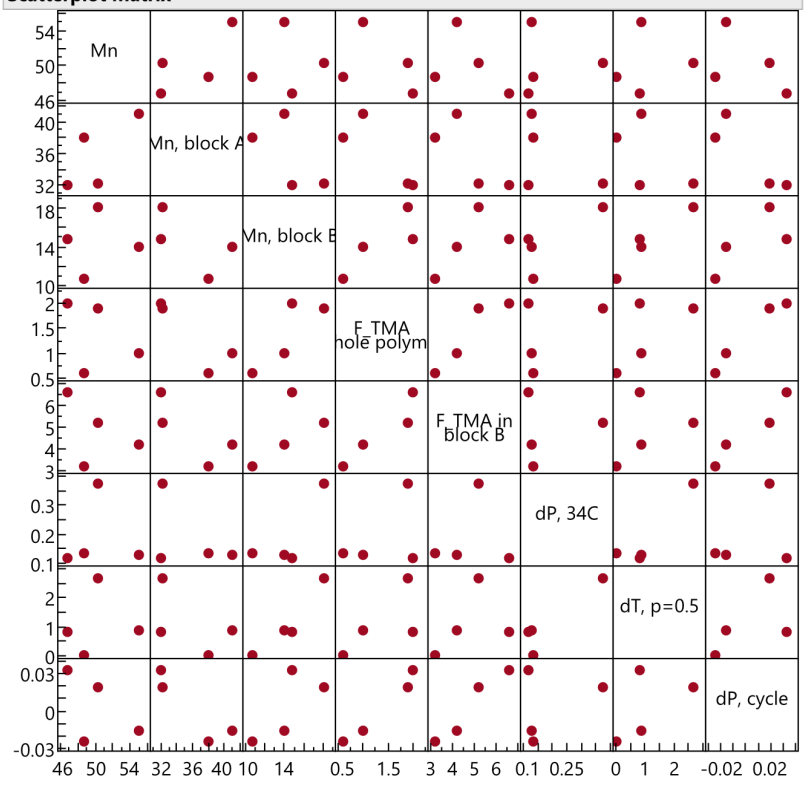

Figure S86: Multivariate analysis shows that hysteresis correlates with B-block molecular weight, where irrecoverable mobility is strongly related to total TMA content

Multivariate

Correlations

	F_TMA whole polymer	F_TMA in block B	dP, cycle
F_TMA whole polymer	1.0000	0.7113	0.9074
F_TMA in block B	0.7113	1.0000	0.3789
dP, cycle	0.9074	0.3789	1.0000

There are 2 missing values. The correlations are estimated by REML method.

Scatterplot Matrix

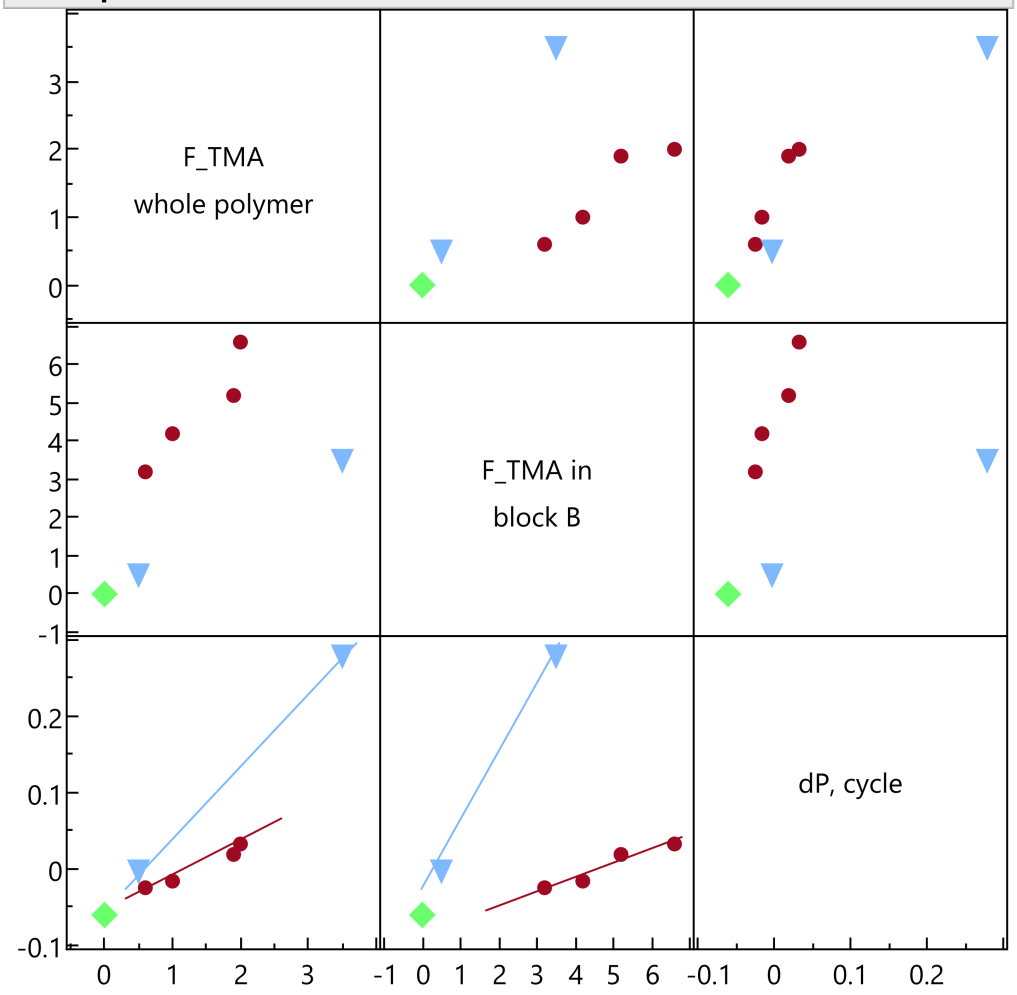

Figure S87: Multivariate analysis shows that blocky-functionalized polymers demonstrate different scaling of irrecoverable mobility with TMA content in the whole polymer and TMA content in the B-block from non-blocky copolymers. Blocky-functionalized polymers shown as maroon triangles, copolymers as blue triangles, and homopolymer as green diamond.

Multivariate

Correlations

	dP, 34C	dT, p=0.5	TCl 1	WC 4
dP, 34C	1.0000	0.9841	-0.9899	0.9755
dT, p=0.5	0.9841	1.0000	-0.9823	0.9919
TCl 1	-0.9899	-0.9823	1.0000	-0.9583
WC 4	0.9755	0.9919	-0.9583	1.0000

There are 3 missing values. The correlations are estimated by REML method.

Scatterplot Matrix

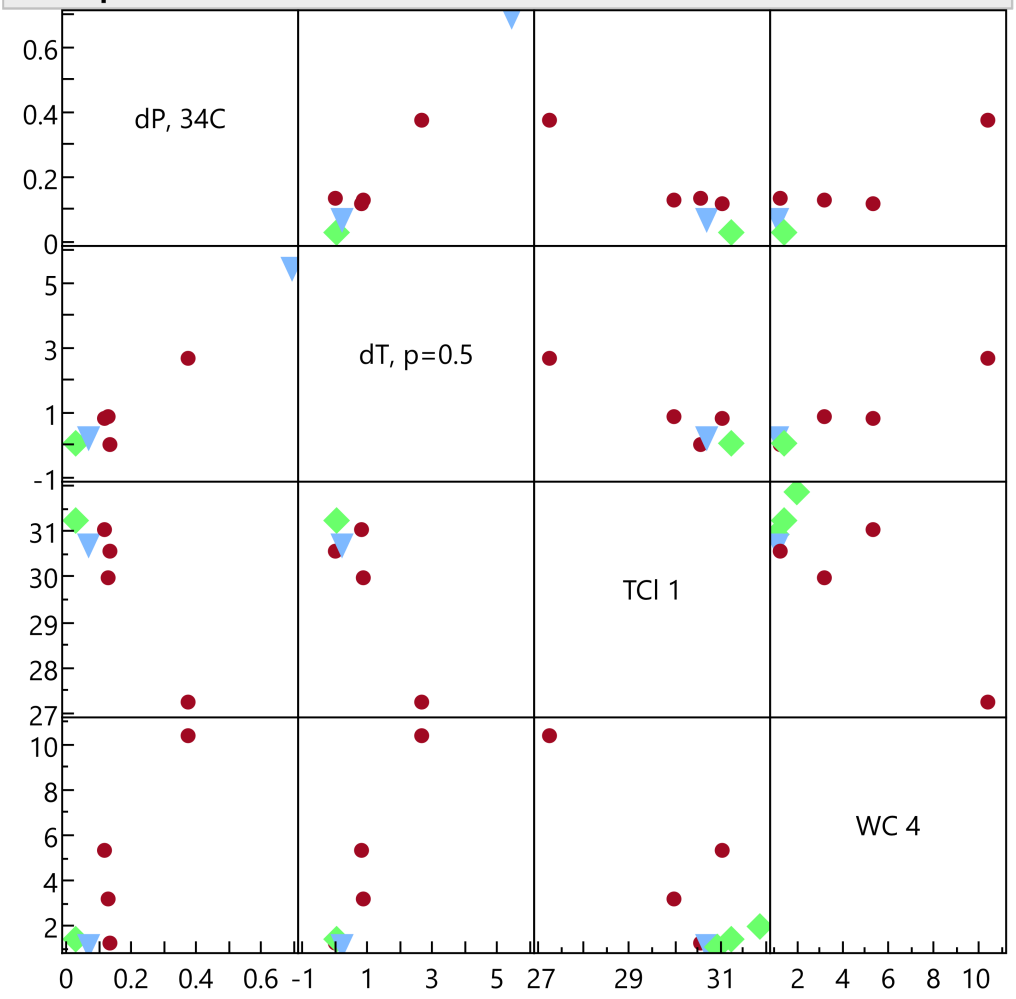

Figure S88: Multivariate analysis shows

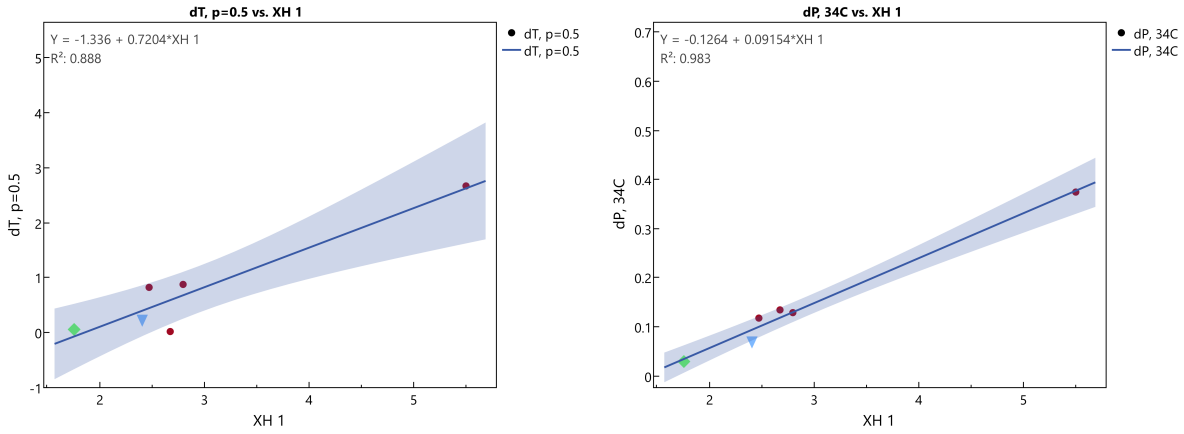

Figure S89: Correlation between hysteresis parameters extracted from VT NMR and CPT

References

[1] G. G. Odian, *Principles of polymerization*, Wiley-Interscience, Hoboken, N.J, 4th edn, 2004.

[2] Z. Osváth and B. Iván, *Macromol. Chem. Phys.*, 2017, **218**, 1600470.

[3] R. E. Hoffman, *Magn. Reson. Chem.*, 2006, **44**, 606–616.

[4] A. Issa and A. Luyt, *Polymers*, 2019, **11**, 537.